Insights into the HER-2 Receptor Tyrosine Kinase Mechanism and Substrate Specificity Using a Transient Kinetic Analysis†

Amy Y. Jan, Eric F. Johnson, A. John Diamonti,‡ Kermit L. Carraway III,‡ and Karen S. Anderson*

Department of Pharmacology, Yale University School of Medicine, 333 Cedar Street, New Haven, Connecticut 06520-8066, and Division of Signal Transduction, Harvard Institute of Medicine, 10th Floor, Beth Israel Deaconess Medical Center, 330 Brookline Avenue, Boston, Massachusetts 02215

Received October 27, 1999; Revised Manuscript Received June 5, 2000

ABSTRACT: The *HER*-2/*erb*B-2/*c-neu* proto-oncogene encodes for an EGF receptor-like protein which has been implicated in the pathogenesis of several human malignancies. Although much has been learned about the physiological significance of this receptor tyrosine kinase, its catalytic mechanism remains poorly understood. We have expressed, purified, and characterized two recombinant proteins corresponding to a full-length (HCD) and truncated (HKD) construct of the HER-2 intracellular tyrosine kinase domain and have identified an optimal substrate (GGMEDIYFEFMGGKKK; HER2Peptide) through screening of a degenerate peptide library. We have conducted a transient kinetic analysis of the HER-2 proteins (HCD and HKD) to illuminate mechanistic details of the HER-2 pathway. In particular, stopped-flow fluorescence studies with mant (*N*-methylanthraniloyl)-nucleotide derivatives provided direct measurements of the association and dissociation rate constants for these nucleotide interactions with the HER-2 recombinant proteins, thereby enabling the determination of nucleotide K_d values. Moreover, the actual step of chemical catalysis was isolated using rapid chemical quench techniques and shown to occur approximately 3-fold faster than the steady-state rate which corresponds to product release. Evidence is also provided that suggests a conformational change that is partially rate-limiting at least in HCD. Furthermore, the role that the phosphorylation state of the protein may play on catalysis was examined. Studies carried out with pre-phosphorylated recombinant HER-2 proteins suggest that while autophosphorylation is *not* a prerequisite for enzymatic activity, this protein modification actually directly affects the catalytic mechanism by enhancing the rate of ADP release and that of the rate-limiting step. While a pre-steady-state kinetic analysis has been carried out on the catalytic subunit of cAMP-dependent serine/threonine kinase, to our knowledge, this study represents the first reported transient kinetic investigation of a receptor tyrosine kinase. This work serves as a basis for comparison of these two important protein kinase families and in this report we highlight these similarities and differences.

The family of known protein kinases comprises a rapidly expanding group of enzymes that mediate diverse cellular functions through the phosphorylaton of protein targets. As determined by their substrate specificities, protein kinases fall into two main categories: protein serine/threonine kinases (PSK)[1] and tyrosine kinases (PTK). Despite their discrimination for amino acid substrates, PSKs and PTKs share significant primary and tertiary homology in their catalytic domains (*2*, *3*). Recently, the structures for a dozen unique kinases distributed approximately equally over both classes have been determined crystallographically (*4*−*15*) and show that the catalytic cores of protein kinases consist of a highly conserved bilobal structure sandwiching a deep cleft in which catalysis occurs. Ternary complexes solved in the presence of nucleotide and peptide substrates support the mechanism of a general-base-catalyzed phosphoryl group transfer at the active site. Although the arsenal of protein kinase structural, biochemical, cellular, and genetic information is expanding at a phenomenal rate, very little is known about the kinetic mechanism(s) by which protein kinases act.

In contrast to steady-state kinetic analysis which primarily provides information on the slowest step in the overall reaction pathway, a transient kinetic analysis can establish the kinetic pathway directly and identify the rate-limiting step in the overall pathway. Moreover, this type of analysis will allow one to observe reactions at the active site of the enzyme including transiently formed enzyme intermediates and changes in protein conformation. Only in recent years has the kinetic pathway for the catalytic subunit of cAMP-dependent serine/threonine protein kinase (cAPK) been elucidated (*16*−*19*) using a transient kinetic analysis.

Using a transient kinetic approach and rapid chemical quench methodology, the phosphorylation of the Kemptide peptide substrate (LRRASLG) was initially determined to occur via a three-step mechanism: substrate binding (K_d =

† This work was supported by ACS RPG-98-027-01 CDD to K.S.A. and Medical Scientist Training Program NIH GM07205 for A.Y.J. and NCI CA71702. to K.L.C.

* To whom correspondence should be addressed. E-mail: karen.anderson@yale.edu. Phone: (203) 785-4526. Fax: (203) 785-7670.

‡ Division of Signal Transduction.

[1] For the rest of this work and unless otherwise specified, "HER-2" will be used to refer to the human version of the receptor, whereas "neu" will refer specifically to the rat protein.

10.1021/bi9924922 CCC: $19.00
Published on Web 07/20/2000

Scheme 1: Schematic of the (A) Full-Length HER-2 Protein, and Recombinant HER-2 Proteins, (B) HKD, and (C) HCD

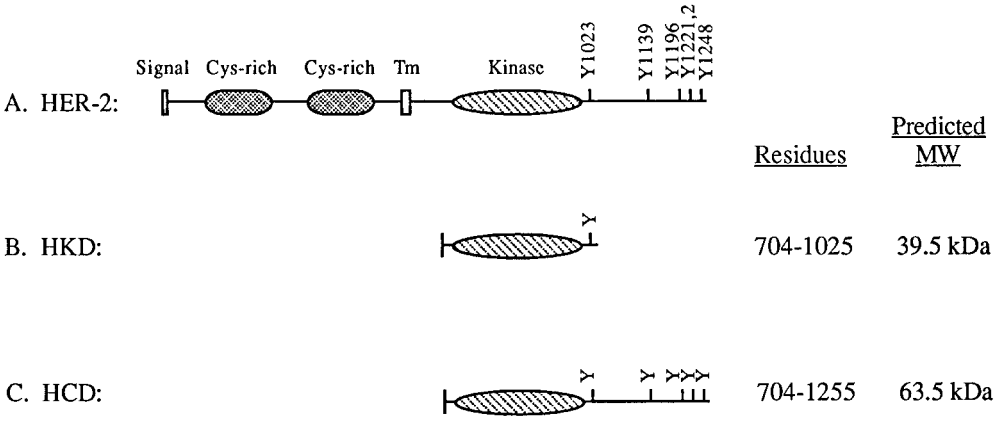

200 ± 50 μM), followed by rapid phosphoryl transfer (500 ± 60 s^{-1}), and a slower product-release step corresponding to the steady-state rate (21 s^{-1}) (*16*). Subsequently, stopped-flow fluorescence studies on an acrylodan-labeled derivative of this enzyme assigned a rate of 100 s^{-1} to the dissociation rate constant for ADP and also provided evidence suggestive of the existence of a partially rate-limiting conformational change occurring after chemical catalysis and prior to product release (*17*). More recent studies have provided further transient kinetic data supporting the existence of partially rate-determining conformational changes along the cAPK pathway (*18*, *19*). These pre-steady-state studies for the catalytic subunit of cAPK have been seminal for understanding the mechanism of substrate phosphorylation catalyzed by this serine/threonine kinase. Until now, however, no receptor tyrosine kinase has ever been analyzed to examine the kinetic processes that are occurring at the enzyme active site. While there are many similarities between these two classes of protein kinases, there are also some distinct differences.

At a cellular level, activation of tyrosine kinases serves as the initial event in the response of cells to extracellular growth factors, and the ensuing relay of phosphorylations and protein−protein interactions ultimately affect cellular processes such as growth and differentiation. Perturbations of these pathways often lead to deregulation of normal cellular growth and the development of malignancies or other proliferative diseases (*20*). Among the most frequently altered gene products in human solid tumors is the human HER-2 receptor, which is found in multiple tumor types including melanoma (*21*) as well as overexpressed in 25−30% of mammary and ovarian carcinomas and associated with poor patient prognosis (*22*−*27*). The HER-2/*neu*[1,2] protein belongs to the EGF receptor/class I family of receptor tyrosine kinases (RTKs), members of which share approximately 60−80% identity in the intracellular tyrosine kinase domain (*1*, *2*, *28*−*34*). Molecular and cellular biological studies have demonstrated the necessity of this tyrosine kinase activity for cellular transformation of HER-2 expressing cells (*35*−*37*). Given its involvement in human cancers, HER-2 has received much attention as a possible target for pharmacological intervention, and the rationale for directing treatment efforts at HER-2 has been substantiated by the success and FDA approval of an anti-HER-2 antibody (Herceptin) (*38*, *39*) in the treatment of HER-2 overexpressing advanced breast cancers. Despite the promising results achieved by Herceptin on tumor growth, patients with significant levels of interfering circulating HER-2 extracellular domain often fail to attain desired serum antibody trough levels (*38*, *40*). Hence, targeting the tyrosine kinase domain itself may provide a complementary treatment strategy for HER-2 bearing tumors. Especially in the absence of three-dimensional structural data for this kinase, a thorough evaluation of the kinetic behavior of the HER-2 tyrosine kinase domain is imperative for understanding the activity of this kinase on a mechanistic level. Furthermore, this information may prove crucial for the successful development of potential chemotherapeutics targeted at this domain through rational drug design.

This paper describes the pre-steady-state kinetic characterization of the human HER-2 tyrosine kinase domain through transient kinetic methodologies. Two HER-2 recombinant proteins were prepared (see Scheme 1) and used for these studies in order to elucidate how residues carboxyl-terminal (C-terminal) to the core kinase domain might impact on catalysis: (1) HKD (HER-2 kinase domain), encompassing core kinase residues Gly 704[3] to Val 1025; and (2) HCD (HER-2 cytoplasmic domain), consisting of residues Gly 704 to Val 1255 which corresponds to all of the residues in HKD as well as the remaining residues of the cytoplasmic tail. *N*-methylanthraniloyl (mant) fluorescent derivatives of the non-hydrolyzable ATP analogue AMP-PNP as well as of ADP were synthesized for stopped-flow fluorescence spectroscopic analyses of nucleotide binding. In addition, rapid quench technologies and [γ−^{32}P]ATP were employed to examine the direct transfer of the gamma-phosphate from

[2] Abbreviations: ADP, adenosine 5′-diphosphate; AgII, angiotensin II; AMP-PNP, 5′-adenylylimidodiphosphate; ATP, adenosine 5′-triphosphate; BSA, bovine serum albumin; C-terminal, carboxyl-terminal; C-terminus, carboxyl-terminus; cAMP, adenosine cyclic 3′,5′-monophosphate; cAPK, cAMP-dependent serine/threonine protein kinase; CDP, cytidine 5′-diphosphate; CV, column volume; ECD, extracellular domain; EDTA, ethylenediaminetetraacetic acid; EGF(R), epidermal growth factor (receptor); GDP, guanosine 5′-diphosphate; GTP, guanosine 5′-triphosphate; HCD, HER-2 cytoplasmic domain; HER-2, human epidermal growth factor receptor; HKD, HER-2 kinase domain; IRS-1, insulin receptor substrate-1; Me^{2+}, divalent metal ion; mant, *N*-methylanthraniloyl; MIA, *N*-methylisatoic anhydride; MOI, multiplicity of infection; Ni^{2+}-NTA, nickel-nitrilotriacetic acid; Nt, nucleotide; PSK, protein serine kinase; PTK, protein tyrosine kinase, PTB, phosphotyrosine-binding domain; RTK(s), receptor tyrosine kinase(s); SDS−PAGE, sodium dodecyl sulfate−polyacrylamide gel electrophoresis; SH2, src homology 2; TLC, thin-layer chromatography; Tris, tris[hydroxymethyl]aminomethane; UDP, uridine 5′-diphosphate;

[3] References to HER-2 sequence are based on that reported by Coussens et al. (*1*).

ATP to the tyrosine of an optimal peptide substrate, HER2Peptide (GGMEDIYFEFMGGKKK) identified through degenerate peptide library screening. These studies have also lead to the identification of a potent peptide inhibitor of HER-2.

The transient kinetic studies using rapid chemical quench allowed the isolation of the chemical catalysis step which was shown to occur 3-fold faster than steady-state rate. Evidence is also provided for the existence of a rate-limiting conformational change. Furthermore, HER-2 autophosphorylation was shown to enhance the rates of ADP release and that of the rate-limiting step. While a pre-steady-state kinetic analysis has been carried out on the catalytic subunit of cAMP-dependent serine/threonine kinase (cAPK), to our knowledge, this is the first reported transient kinetic investigation of a receptor tyrosine kinase. This work serves as a basis for comparison of these two important protein kinase families and in this report we highlight similarities and differences between the two classes of enzyme protein kinases.

MATERIALS AND METHODS

Materials. Bac-to-Bac baculovirus expression system, Sf900 II SFM media, rTEV protease, *Spodoptera frugiperda* (Sf9) cells, and penicillin-streptomycin were from Gibco BRL. pGEM clone 0483 was a generous gift of Genentech. Ni^{2+}-NTA Superflow resin was from Qiagen. Rabbit anti-HER-2 polyclonal antibodies SC-O7 (raised against core kinase residues 866−880) and SC-284 (raised against carboxyl tail residues 1169−1186) were from Santa Cruz Biotechnology, Inc. Mouse anti-phosphotyrosine antibody 4G10 was from Upstate Biotechnology, Inc. [γ-^{32}P]ATP (10 mCi/mL), [γ-^{32}P]GTP (10 mCi/mL), enhanced chemiluminescence detection kit and donkey-anti-rabbit/sheep anti-mouse horseradish peroxidase secondary antibodies were from Amersham. Superdex 75 gel filtration column was from Pharmacia Biotech. Gel filtration standards (no. 151−1901), P-6 Biospin chromatography columns, and Bio-Rad Protein Assay were from Bio-Rad. Cellulose PEI, F-254 thin-layer chromatography plates were from Selecto Scientific. Adenosine 5′-triphosphate (ATP), adenosine 5′-diphosphate (ADP), 5′-adenylylimidodiphosphate (AMP-PNP), guanosine 5′-triphosphate (GTP), guanosine 5′-diphosphate (GDP), cytidine 5′-diphosphate (CDP), sodium orthovanadate, uridine 5′-diphosphate (UDP), [Val^5]-angiotensin II ([Val^5]AgII) (DRVYVHPF) and [Ile^5]-angiotensin II ([Ile^5]AgII) were obtained from Sigma. HER2Peptide (GGMEDIYFEFMGGKKK) and DNA primers were synthesized by the DNA and peptide synthesis facilities, respectively, at the W. M. Keck Biotechnology Resource Center at Yale University, New Haven, CT. Nucleotide concentrations were determined spectroscopically using extinction coefficients (ϵ) as follows: $\epsilon_{259} = 15.4$ mM^{-1} cm^{-1} for adenosine nucleotides; $\epsilon_{253} = 13.7$ mM^{-1} cm^{-1} for guanosine nucleotides; $\epsilon_{271} = 9.1$ mM^{-1} cm^{-1} for CDP; and $\epsilon_{262} = 10.0$ mM^{-1} cm^{-1} for UDP. Peptide concentrations were estimated based on their tyrosine content using an extinction coefficient at 280 nm of 1.4 mM^{-1} cm^{-1}. Highly pure *N*-methylisatoic anhydride (MIA) was from Molecular Probes. ATP, AMP-PNP, ADP and silica gel 60, F_{254} TLC plates were from Sigma. mantATP was a generous gift from Dr. Kenneth A. Johnson (University of Texas, Austin).

Construction and Isolation of Recombinant Baculoviruses. Our initial attempts to produce active HER-2 recombinant proteins in bacteria and yeast were unsuccessful because of insolubility and inadequate yields, respectively. Therefore we turned our efforts to the development of a baculovirus protein expression system. Recombinant baculoviruses were constructed using the Bac-to-Bac system (Gibco BRL) for the expression of recombinant HER-2 proteins with rTEV protease cleavable amino-terminal His-tags. Construct HKD carries HER-2 sequences corresponding to core kinase domain amino acid residues Gly 704 to Val 1025, and construct HCD encodes HER-2 cytoplasmic domain amino acid residues Gly 704 to Val 1255 (Scheme 1). Briefly, pGEM clone 0483 (Genentech) encoding the full-length human *HER*-2 cDNA served as a template for PCR-based cloning (5′ forward primer, 5′ AATATAAACGGTCCGGCGCCATGCCCAACCAGGCGCAGATG 3′; HKD 3′ reverse primer, 5′ ATAATTTAGCGGCCGCTCATACCAGATACTCCTCAGCATC 3′; HCD 3′ reverse primer, 5′ ATAATTTAGCGGCCGCTACGTATCACACTGGCACGTCCAGACCCAG 3′) of the *HER*-2 cytoplasmic domains into the *Nar*I and *Not*I multiple cloning sites of pFastBacHTa donor plasmid under transcriptional control of the polyhedrin promoter (Gibco BRL). Positive subclones were identified by restriction enzyme digestion and sequenced to confirm sequence integrity. Subsequent generation of recombinant baculovirus from each recombinant pFastBacHTa donor plasmid was performed according to manufacturer protocols (Gibco BRL).

Purified recombinant viruses were amplified with two rounds of infection in Sf9 cells grown in suspension in Sf900 II SFM media (Gibco BRL) supplemented with penicillin-streptomycin (to 25 units of penicillin and 25 mg of streptomycin/mL of media) at 2.0×10^6 cells/mL at 28 °C using a multiplicity of infection (MOI) of 0.1. Virus-containing supernatants were harvested approximately 36 h post-infection and titered.

Purification of Recombinant HER-2 Proteins. For protein expression, time course studies were performed at various MOIs to establish the following optimal expression parameters. Sf9 cells were grown in suspension at 28 °C to a density of 3.0×10^6 cells/mL and infected at an MOI of 1. When cell viability decreased to approximately 80% (40−50 h postinfection), cells were collected by centrifugation at 500$g \times$ 10 min, gently washed with cell suspension buffer (20 mM Hepes−Na, pH 7.5, 4 mM $NaHCO_3$, 55 mM KCl, 5 mM $CaCl_2$, and 78 mM Sucrose) (*41*), repelleted to remove excess supernatant, frozen with liquid nitrogen, and then stored at −80 °C until use.

All steps of the protein purification were carried out at 4 °C and completed within 34 h after cell lysis. Initial attempts at purification were repeatedly foiled by protein precipitation until Tween-20 was included at ≥0.01%. Cell pellets were resuspended in 5 mL of lysis buffer/g of cell pellet (50 mM Tris-HCl, pH 8.5 at 4 °C, 150 mM NaCl, 1% Tween-20, 20% glycerol, 10 mM β-ME, 4 mM benzamidine, 5 μg/mL aprotinin, 5 μg/mL leupeptin, 2 mM pepstatin A, 1 mM phenylmethanesulfonyl fluoride) and tumbled end-over-end at 4 °C for 1.5 h. The cell lysate was then centrifuged at 39000$g \times$ 45 min at 4 °C, and the supernatant was then incubated with Qiagen Ni^{2+}-NTA (nickel-nitrilotriacetic acid) Superflow resin and tumbled at 4 °C × 1.5 h. A column

volumn (CV) of approximately 0.4 mL (for HKD) or 0.14 mL (for HCD) of Ni^{2+}-NTA resin was used per liter of insect cell growth harvested. The Ni^{2+}-NTA-bound proteins were washed in series by batch purification (with tumbling at 4 °C × 5 min followed by 2 min centrifugation at 1000*g* for each step) with the following solutions: 7 × 5 CV of 5 mM imidazole in Wash A (20 mM Tris-HCl, pH 8.5 at 4 °C, 100 mM KCl, 20% glycerol, 10 mM β-ME, 0.05% Tween-20), 1 × 2 CV Wash B (20 mM Tris-HCl, pH 8.5 at 4 °C, 1 M KCl, 20% glycerol, 10 mM β-ME, 0.05% Tween-20), 1 × 2 CV 10 mM imidazole in Wash A, and 1 × 2 CV 20 mM imidazole in Wash A. Recombinant proteins were then eluted with 3 × 3 CV of 110 mM imidazole (for HKD) or 60 mM imidazole (for HCD) in Wash A. Proteins were concentrated to approximately 1 mL using Centricon-30 concentrators (Amicon, Inc.) prior to further purification on a 120 mL Sephadex-75 Gel Filtration column (Pharmacia) eluted with 100 mL of enzyme storage buffer (20 mM Tris-HCl, pH 7.9 at 25 °C, 100 mM NaCl, 20% glycerol, 5 mM DTT, 0.01% Tween-20). Proteins were then concentrated to two convenient stock concentrations ranging from 20 to 50 μM and 200 to 500 μM, frozen with liquid nitrogen, and stored at −80 °C. Protein concentrations were estimated by Bio-Rad protein assay using bovine serum albumin (BSA) as standard. For all studies, enzyme aliquots were then thawed only once for immediate use.

Western Blot Analysis. Proteins were resolved by sodium dodecyl sulfate−polyacrylamide gel electrophoresis (SDS−PAGE) (*42*) and transferred to nitrocellulose membranes using a Bio-Rad Mini Trans-Blot cell according to manufacturer protocols. For blots probed with rabbit-anti-HER-2 antibodies SC-07 or SC-284 (Santa Cruz Biotechnology, Inc.), nitrocellulose membranes were first blocked overnight at 4 °C in blotto [5% (w/v) milk dissolved in Tris-buffered saline (TBS)]. SC-07 (diluted 1:1000 in blotto) or SC-284 (diluted 1:10000 in blotto) was then added for 1 or 2 h at room temperature, respectively. Blots were then washed with two 5 min exchanges of TBS-T (TBS supplemented with Tween-20 to 0.1%) followed by TBS. Donkey-anti-rabbit horseradish peroxidase-conjugated secondary antibody was then diluted 1:5000 in blotto and added to membranes for 2 h at room temperature. After a second series of washes as described above, immunoreactive bands were visualized with the Amersham enhanced chemiluminescence system. Immunoblots probed with mouse anti-phosphotyrosine antibody 4G10 (Upstate Biotechnology, Inc.) were conducted essentially the same as for SC-284, except that 5% BSA in TBS-T2 (TBS supplemented with Tween-20 to 1%) was used instead of blotto and that a sheep-anti-mouse antibody was used as the secondary antibody.

Synthesis of 2′(3′)-O-(N-Methylanthraniloyl)−Nucleotide Analogues. N-Methylanthraniloyl (mant) derivatives of AMP-PNP and ADP were synthesized by reaction with *N*-methylisatoic anhydride (MIA) (Molecular Probes) according to the method of (*43*) except that a Q-Sepharose Fast-flow column (Pharmacia) was used to purify the analogues after the reaction. Specifically, 3.5 mL of a 66.7 mM nucleotide solution (0.23 mmol) dissolved in water was adjusted to pH 9.6 with 1 N NaOH at 38 °C. 1.5 M equiv of crystalline MIA was slowly added, and pH maintained at ∼9.6 by titration with 1 N NaOH. After completion of the reaction (determined by stabilization of pH and dissolution of MIA, generally occurred after ∼2 h), the solution was readjusted to pH 7.6 with 1 N HCl and applied to a 20 mL column volume (CV) Q-Sepharose column. The column was eluted with a linear gradient of 10 mM to 0.6 M triethylammonium bicarbonate, pH 7.5 over 20 CV. The fluorescent nucleotides eluted after and well-resolved from the reactants. Pooled fractions were lyophilized to dryness, and the remaining triethylamine was removed by three additions and rotary evaporations of methanol. Purity of mantADP and mantAMP-PNP was analyzed by thin-layer chromatography (TLC) using silica gel 60, F_{254} developed with 2-propanol/NH_4OH/water (7:1:2, v/v/v) (*44*). The spectrophotometric properties of all analogues were tested, and the A_{255}/A_{356} ratios for 2′(3′)-mantAMP-PNP and 2′(3′)-mantADP were approximately 4, indicating that the derivatives obtained were monosubstituted (*45*). The extinction coefficients of mantATP have been reported as $\epsilon_{255} = 23.2\ mM^{-1}\ cm^{-1}$ and $\epsilon_{356} = 5.7\ M^{-1}\ cm^{-1}$ (*43*), hence, these values were used to determine the concentrations of the mant-adenosine nucleotide analogues.

Tyrosine Kinase Assays. Kinase assays were typically performed at 25 °C and initiated by mixing a 2× enzyme solution (∼10 μM, diluted in enzyme storage buffer) 1:1 with a 2× substrate solution [2−200 μM [γ-^{32}P]ATP (0.5−50 mCi/mmol), 20 mM $MnCl_2$, 20 mM Tris-HCl, pH 7.4 at 25 °C, 100 μM Na_3VO_4]. For exogenous peptide phosphorylation, the 2× enzyme solutions were supplemented with the relevant peptide such that final concentrations in the 1× reaction mixture were as indicated in the text. To determine the nucleotide inhibition constants (K_i), 10 μM or 20 μM of mantADP, ADP, mantAMP-PNP, or AMP-PNP were included in steady-state type competition experiments with four different concentrations of ATP.

The reactions were manually quenched after noted time periods (typically 10−1200 s) with EDTA to a final concentration of 200 mM. Zero time points were determined by addition of EDTA to the 2× Enzyme solution prior to mixing with 2× substrate solution. Radioactive bands corresponding to ATP, phosphorylated enzyme, and phosphorylated peptide were resolved on 15 or 18% SDS−polyacrylamide gels and quantitated by phosphorimager analysis (*42*). Unless otherwise indicated, final 1× reaction concentrations for enzymes and substrates will be subsequently reported for these studies. For ease of discussion, enzyme concentrations are reported in terms of molarity as determined from Bio-Rad protein assays using BSA as standard. Unless otherwise indicated, initial reaction rates were determined from reaction time courses by plotting the amount of phosphorylated product formed over time, fitting the data to a single exponential using nonlinear regression methods in KaleidaGraph, and then differentiating the resulting curve at time zero seconds.

Likewise, for the determination of nucleotide K_i values, the initial rates (V) at each ATP concentration in the presence/absence of the various competing nucleotides could then be fit by nonlinear regression to a hyperbola [$(V = V_{max}[ATP])/(K_{m,app} + [ATP])$] using KaleidaGraph to determine the apparent Michaelis constant ($K_{m,app}$). Corresponding Lineweaver−Burke reciprocal plots were also made for each nucleotide condition. The K_i for each competing nucleotide was then determined from either or both of the following replots: $K_{m,app}$ (ordinate) versus [competing nucleotide]

(abscissa: 0, 10, 20 μM); or, slope obtained from Lineweaver−Burke plot (ordinate) versus [competing nucleotide] (abscissa). For either method, the intercept on the abscissa determined from a linear fit of the data is equal to $-K_i$ (*73*).

Degenerate Peptide Library Screen. The substrate preference of the HER-2 kinase domain was determined using a degenerate peptide library according to published protocols (*46*, *47*). This library consists of 15-mer peptides which all contain a single tyrosine at residue 7 flanked on both sides by four degenerate positions to yield the following sequence: Met-Ala-X-X-X-X-Tyr-X-X-X-X-Ala-Lys-Lys-Lys, where X indicates all amino acids except tryptophan, cysteine, tyrosine, serine, or threonine. The recombinant HER-2 proteins were added to the peptide library under conditions such that 2−5% of the peptides became phosphorylated (5% in the screen conducted with HCD; 2% in the screen conducted with HKD). More specifically for HCD, 5 μM HCD was incubated with 150 μM ATP and 1.3 mg/mL peptide library (~770 μM, assuming an average peptide molecular mass of 1700 Da) for 25 min. For HKD, 1 μM HKD was incubated with 100 μM ATP and 1.3 mg/mL peptide library for 12 min. Other reaction components were as described above. The phosphopeptide products were then separated from the HER-2 kinases using a microcon-30 concentrator (Amicon, Inc.), quantitatively purified from the nonphosphorylated peptides using a ferric iminodiacetic acid column and sequenced. Comparison of the amino acid abundance at each degenerate position in the phosphopeptide pool relative to that at the same position in the starting mixture provided a selectivity profile for HER-2 at these locations.

Steady-State Assay To Assess Inhibition of Truncated Peptides. The steady-state inhibition assays were initiated by addition of HKD enzyme (final concentration of 2 μM) to a substrate mix containing all other reaction components to give the following: 10 mM $MnCl_2$, 25 mM TrisHCl pH 8.0 at RT, 2 μM ATP, 0.05 μCi/μL γ-^{32}P-ATP, 0.03% BSA, 4% DMSO, 25−500 μM peptide substrate (HCDpeptide), 0−500 μM 13mer peptide (HCD-13mer). The reaction was allowed to proceed for 75 s at 25 °C before quenching with a final concentration of 0.2 M EDTA.

Preparation of Self-Phosphorylated ^{32}P·HER-2 Recombinant Proteins. Approximately 20 μM HKD or HCD was self-phosphorylated in reaction mixtures containing 10 mM $MnCl_2$ and 100 μM [γ-^{32}P]ATP (for HKD) or 150 μM [γ-^{32}P]ATP (for HCD) for 10 min at room temperature. Other reaction components were as previously described in "Tyrosine Kinase Assays". Excess nucleotides were removed by serial application on three P-6 Biospin chromatography columns preequilibrated with enzyme storage buffer. To determine the extent of self-phosphorylation and the resulting specific activity of the enzyme, aliquots of the original self-phosphorylation reaction were quenched with 0.2 M EDTA and resolved on 15% SDS−polyacrylamide gels followed by phosphor-imager analysis. The concentration of the buffer-exchanged, self-phosphorylated HER-2 protein preparations could then be determined by comparison with gel and phosphor-imager analysis of the P-6 purified autophosphorylation reaction mixture. ≥98% of [γ-^{32}P]ATP was routinely removed using this procedure. Typically, this procedure resulted in a recovery of only ~30% of starting enzyme concentrations.

For the stopped-flow experiments, no radioactive ATP was included in the autophosphorylation reactions. For the rapid chemical quench studies, the autophosphorylation reaction contained 120 μM enzyme and 400 μM ATP. This higher enzyme concentration was necessary in order to achieve the 10 μM final concentration desired for these experiments because of incomplete recoveries during the preparation of the self-phosphorylated enzyme. Final concentrations during mixing in the rapid chemical quench were 2 mM HER2Peptide, 9.9 μM ^{32}P-HKD and 100 μM [γ-^{32}P]ATP.

^{32}P·HER-2 Dephosphorylation Assays to Examine the Reverse Reaction. Self-phosphorylated ^{32}P-HKD or ^{32}P-HCD (2 μM) was incubated at 25 °C with 1−100 μM ADP, 10 mM $MnCl_2$, 20 mM Tris-HCl, pH 7.4, and 50 μM Na_3VO_4. After various time periods, the reactions were quenched with 0.2 M EDTA. In cases where alternative nucleotides were used, 100 μM GDP, CDP or UDP was included in the reaction solutions in lieu of ADP. The extent of ^{32}P·HER-2 dephosphorylation and concomitant [γ-^{32}P]ATP formation was monitored by phosphor-imager anaylsis of reaction products resolved by SDS−PAGE. In addition, separation of the reaction products on PEI-cellulose thin-layer chromatography plates developed with 0.6 N KPO_4, pH 3.4, verified the generation of [γ-^{32}P]ATP from ADP.

Probing for the Existence of a Phospho−Enzyme Intermediate. Self-phosphorylated ^{32}P·HER-2 proteins prepared as above were mixed 1:1 with 2× Substrate solutions containing 100 μM of the indicated nucleotide (AMP-PNP, ADP, or ATP) and/or 5 mM [Val^5]AgII. Other reaction components were as previously described for "Tyrosine Kinase Assays". Reactions were allowed to proceed for 30 min at 25 °C before being quenched with EDTA at a final concentration of 0.2 M. Products were resolved on 15% polyacrylamide gels and visualized with phosphor-imager analysis.

Data Analysis. As indicated above, all curve fitting was performed using nonlinear regression methods provided by the KaleidaGraph computer program. Initial reaction rates were typically determined from reaction time courses (using four to six nonzero time points) by plotting the amount of phosphorylated product (P) formed over time, fitting the data to the single-exponential equation $[P] = A(1 - \exp(-kt))$, and then differentiating the resulting curve at time zero seconds (which for this equation is mathematically equivalent to the product, kA). When the curve of product formation over time was better approximated by a line (as opposed to a single exponential), the curve was fit to the equation $[P] = mx + b$ and the initial reaction rate was then determined from the slope (m) of the resulting line. The initial reaction rates were then plotted as a function of substrate concentration and fit to the various equations noted within the text.

Stopped-Flow Fluorescence Spectroscopy. Stopped-flow experiments were performed using a KinTek StopFlow System (model SF-2001, KinTek Corp., State College, PA). The stopped-flow apparatus allows for the rapid mixing of two solutions (e.g., one containing enzyme, the other containing substrate), which then flow into an observation cell where the reaction can be monitored over time periods as short as 1.5 milliseconds. An excitation wavelength of 290 nm was used to excite enzyme-bound mant fluorophore by way of fluorescence energy transfer from tryptophan and/or tyrosine residues present in the HER-2 recombinant

proteins. Fluorescence emission from the mant-nucleotides was monitored using a 450 nm interference filter. Traces typically represent the average of 3−7 stopped-flow transients. Measurements were performed at room temperature in enzyme storage buffer (20 mM Tris-HCl, pH 7.9 at 25 °C, 100 mM NaCl, 20% glycerol, 5 mM DTT, 0.01% Tween-20) supplemented with $MnCl_2$ to 10 mM. Unless otherwise specified, all concentrations represent final values after mixing. In most experiments, an average of four runs was used for data analysis and a minimum of a 5-fold excess of the variable substrate over enzyme was used to allow analysis as a pseudo-first-order rate constant.

For mantAMP-PNP or mantADP binding, 0.75 μM HCD or HKD was rapidly mixed with increasing concentrations of the mant-nucleotide (7.5−120 μM). The resulting fluorescence (F) time courses were then fit to equations describing a single exponential using the KinTek software to obtain rate constants (k_{obs}) for nucleotide association:

$$F = A \exp(-k_{obs}t) + C$$

where F is a measure of fluorescence intensity in arbitrary units, A is the amplitude of the curve, and C is a constant. To examine the release of bound mantAMP-PNP or mantADP from the HER-2 proteins, 2−2.5 μM HKD or HCD was preincubated with 10 μM of the mant-nucleotide at room temperature for 15 min. The HER-2•mant-nucleotide complex was then rapidly mixed with an excess of ATP or AMP-PNP (0.5 or 1 mM), and dissociation rate constants were determined by fitting the traces to single-exponential decay curves using the KinTek software. To ensure that the mant-nucleotides did not dissociate from the HER-2•mant-nucleotide complex as a result of the mere effects of dilution, the concentration of these fluorescent analogues was kept constant by including the compounds (10 μM) in both stopped-flow sample syringes.

Rapid Chemical Quench Measurements. Rapid quench experiments were performed using a KinTek RFQ-3 Rapid Chemical Quench Apparatus (KinTek Corporation, State College, PA) at 25 °C. Typically, the reaction was initiated by mixing a solution containing peptide and enzyme (15 μL) with a solution containing [γ-^{32}P]ATP and $MnCl_2$ (15 μL). Unless otherwise noted, concentrations cited in the text are those after mixing and during the enzymatic reaction. For these experiments, reactant concentrations used were 10 μM HCD or HKD or 9.9 μM prephosphorylated HKD, 2 mM HER2Peptide, 100 μM [γ-^{32}P]ATP (0.5 mCi/mmol), 10 mM $MnCl_2$, 20 mM Tris-HCl, pH 7.4, at 25 °C, 10% glycerol, and 0.005% Tween-20. After various reaction times (25−4000 ms), the reaction mixture was terminated with 67 μL of 0.3 M EDTA (for a final concentration of 200 mM). Radioactive substrates and products were resolved on 18% SDS−polyacrylamide gels (*42*) and quantitated by phosphor-imager analysis. Zero time points were determined by addition of EDTA to the enzyme solution prior to mixing with substrate solution.

Data in each rapid quench time course were fit to a burst equation by nonlinear regression methods using KaleidaGraph:

$$y = A(1 - \exp(-k_b t)) + V_{ss}t$$

where A is the observed "burst" amplitude, k_b is the observed single-exponential "burst" rate constant, and V_{ss} is the observed linear steady-state rate of product formation.

RESULTS

Expression and Purification of Recombinant HER-2 Tyrosine Kinase Domains. To study the in vitro tyrosine kinase activity of HER-2 and examine the potential impact of the C-terminal tail on catalysis, two recombinant proteins (Scheme 1) corresponding to the kinase (HKD) and full-length cytoplasmic (HCD) domains of the receptor were expressed using a baculovirus expression system as described in the Materials and Methods. Western blots of recombinant baculovirus-infected insect cell lysates probed with anti-HER-2 antibodies SC-07 and SC-284 (Santa Cruz Biotechnology, Inc.) identified unique immunoreactive bands of expected sizes (data not shown). Purification of the His-tagged recombinant proteins on Ni^{2+}-NTA resin followed by gel filtration chromatography typically yielded ∼1.5 mg HKD and ∼0.5 mg of HCD/L of insect cell growth. Elution of HKD from the gel filtration step typically occurred at a concentration of ∼40 μM with an apparent molecular mass of ∼37 kDa, while HCD eluted at a concentration of ∼15 μM and apparent molecular mass of ∼126 kDa. From Coomassie blue stained polyacrylamide gels, preparations were ∼98% pure, with HKD migrating at ∼37 kDa and HCD at ∼80 kDa (Figure 1A). The molecular mass of the proteins was also verified using electrospray ionization mass spectrometry (data not shown). For each protein (HKD and HCD), the molecular ion observed indicated that the protein isolated from the baculovirus expression system was in an unphosphorylated state. This analysis coupled with immunoblotting data below verifies that the recombinant enzyme isolated from baculovirus is homogeneous and is not phosphorylated on other residues such as serine.

Analysis of purified HKD by gel filtration chromatography is consistent with the monomeric form even at protein concentrations as high as 40 μM (∼2 mg/mL). However, according to the theoretical molecular mass, the elution profile for the purification of the HCD protein is consistent with a monomeric or dimeric form of the protein.

Phosphorylation Status of the Purified HKD and HCD Proteins. To further confirm the phosphorylation status of the recombinant HER-2 proteins upon purification, western blots of HCD and HKD were performed. As can be seen in Figure 1B, panel i (lanes 2 and 4), no immunoreactive bands are detected when the purified HKD or HCD proteins are probed with an anti-phosphotyrosine antibody. It is only after the proteins have been self-phosphorylated with the addition of ATP that immunoreactivity becomes apparent (Figure 1B, panel i, lanes 3 and 5). Probing these samples with anti-HER-2 antibodies reveals immunoreactive bands at expected positions and shows that similar amounts of protein were loaded for samples treated with and without ATP (Figure 1B, panel ii).

Demonstration of Tyrosine Kinase Activity. To determine whether the purified HER-2 proteins are capable of phosphorylating exogenous peptide substrates, we assayed the ability of HKD and HCD to transfer the γ-phosphate from [γ-^{32}P]ATP to the [Val^5]-angiotensin II ([Val^5]AgII) peptide (DRVYVHPF). Phosphor-imager analysis of reaction prod-

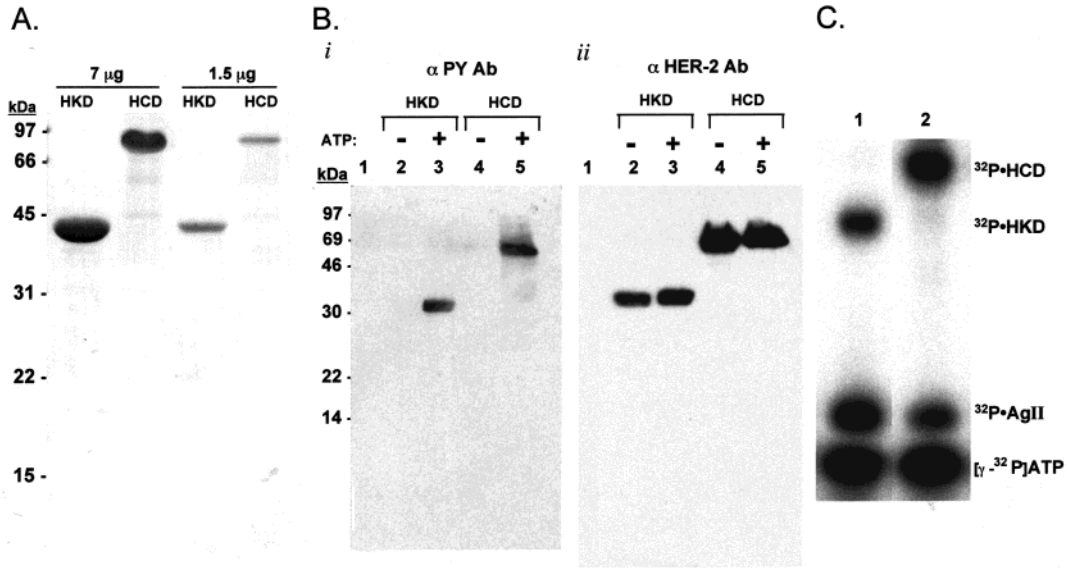

FIGURE 1: (A) Coomassie blue stain of purified HER-2 recombinant proteins. A total of 7 μg (lanes 1 and 2) or 1.5 μg (lanes 3 and 4) of purified HKD (lanes 1 and 3) and HCD (lanes 2 and 4) was resolved on 15% SDS−polyacrylamide gels and visualized with Coomassie blue. (B) Western Blots of HKD and HCD probed with (i) anti-phosphotyrosine antibody 4G10 or (ii) anti-HER-2 antibodies SC-07 and SC-284. A total of 6.3 μM HKD (lanes 2 and 3) or 3.9 μM HCD (lanes 4 and 5) was incubated in the absence (lanes 2 and 4) or presence (lanes 3 and 5) of 100 μM ATP. All reactions were conducted at 25 °C for 20 min in the presence of 10 mM $MnCl_2$, 50 μM Na_3VO_4, and 20 mM Tris-HCl, pH 7.4. A total of 1.2 μg of BSA control (lane 1) or 1.2 μg of protein from each reaction was then loaded for separation on 15% SDS-polyacrylamide gels and transferred to nitrocellulose membranes for immunoblotting. (C) Demonstration of tyrosine kinase activity. A representative image is shown of HKD (lane 1) and HCD (lane 2) phosphorylation events resolved by SDS−PAGE and analyzed on phosphor-imager. Here, reaction mixtures containing 4 μM enzyme, 5 mM AgII peptide and 10 μM [γ-^{32}P]ATP (20 mCi/mmol) were quenched with 0.2 M EDTA after 30 s and resolved on 15% polyacrylamide gels.

ucts resolved by SDS−PAGE revealed radioactive bands with migrations consistent with those expected for ^{32}P•HCD/HKD, ^{32}P•[Val^5]AgII and [γ-^{32}P]ATP (Figure 1C). Radioactive bands were excised and eluted for analysis by HPLC and/or thin-layer chromatography (TLC) to confirm band assignments for [γ-^{32}P]ATP by comparison with elution profiles of known standards (data not shown). The divalent metal ion (Me^{2+}) preference of HCD and HKD for catalysis was examined by determining initial rates of phosphopeptide formation ([Val^5]AgII) in the presence of [γ-^{32}P]ATP at various concentrations of $MnCl_2$ (2.5−10 mM) or $MgCl_2$ (10 mM). Similar to that observed for other receptor tyrosine kinases, at 10 mM Me^{2+}, both proteins utilize Mn^{2+} 5−10-fold more effectively than Mg^{2+} as a cofactor. To allow comparisons of kinetic parameters with other receptor tyrosine kinases and to have optimal enzyme activity, 10 mM $MnCl_2$ was included in all subsequent reactions (*41*, *48*−*51*). This is in contrast to the optimal metal ion requirement for serine/threonine kinases such as cAPK and nonreceptor tyrosine kinases such as v-abl and src that utilize Mg^{2+}more effectively for catalysis (*16*), (*52*).

Steady-State Characterization. Kinetic parameters were measured in the presence of 5 μM enzyme, as determined by Bio-Rad Protein Assay using BSA as standard. This initial steady-state kinetic analysis allows an assessment of the kinetics of our recombinant receptor tyrosine kinase proteins and serves as a basis for comparison with steady-state kinetic analyses that have previously been reported for other receptor tyrosine kinases.

For HER-2 autophosphorylation, the tyrosine substrates are the autophosphorylation sites of the protein. Hence, enzyme concentrations are necessarily stoichiometric with the concentration of autophosphorylation sites. Eventhough the second substrate (ATP) can be varied independently of enzyme concentration for the determination of its steady-state kinetic parameters, this stipulation on the concentration of autophosphorylation sites renders determination of initial rates by conventional methods difficult. In particular, standard initial rate experiments generally require the analysis of product formation over time periods wherein only a small fraction (≤20%) of reactants are turned over. However, phosphorylation of a single autophosphorylation site would result in 20% turnover of known sites in HCD and 100% turnover in HKD. To circumvent the problem of nonlinearity in the range of manually assessable time points, initial rates were determined by following the progress of the reaction (typically 0−1200 s) as it reaches completion and then differentiating the resulting curve at $t = 0$. The initial rates were assessed in the presence of 1−50 μM [γ-^{32}P]ATP (1−50 mCi/mmol) to examine the rate dependence on nucleotide concentration, and the data were fit by nonlinear regression (KaleidaGraph) to a hyperbola $[(V_{max}[ATP])/(K_m + [ATP])]$, to estimate K_m and V_{max} for ATP. Results are summarized in Table 1. Similar K_m values for ATP were also obtained using lower enzyme concentrations (data not shown), but using 5 μM enzyme allows for greater sensitivity for the detection of autophosphorylation events at the higher concentrations of ATP used. For HCD, the K_m for ATP was also measured in the presence of excess [Val^5]AgII (5 mM) by monitoring the rate of total exogenous peptide and self-phosphorylation events over time, and determined to be 9.9 ± 0.4 μM. Thus, the presence of peptide does not significantly affect the apparent K_m of ATP for the HER-2 enzyme. Each HER-2 construct was then characterized for its ability to phosphorylate an exogenous peptide substrate using saturating concentrations of [γ-^{32}P]ATP (50 μM, 1 mCi/mmol) and 160−5000 μM [Ile^5]AgII (Table 1). Although [Ile^5]AgII was used in these studies, preliminary data indicate

Table 1: Steady-State Parameters for HKD and HCD

HER-2 domain	substrate	K_m (μM)[c]	V_{max} (μM s^{-1})[c]
HKD	ATP[a]	2.7 ± 0.4	0.14 ± 0.01
	[Ile^5]AgII[b]	1400 ± 300	0.19 ± 0.01
	HER2Peptide[b]	390 ± 110	0.50 ± 0.04
HCD	ATP[a]	8.8 ± 1.2	0.31 ± 0.01
	[Ile^5]AgII[b]	950 ± 140	0.16 ± 0.01
	HER2Peptide[b]	350 ± 30	0.54 ± 0.02

[a] Reported parameters were obtained using 5 μM enzyme in self-phosphorylation as described in the text. [b] Reported parameters were obtained using exogenous substrate phosphorylation reactions, as described in the text. [c] The steady-state parameters K_m and V_{max} for each indicated substrate were obtained from initial rate determinations at each of four or five substrate concentrations. Each initial rate determination was performed using a time course of four or five nonzero time points, as described in the Materials and Methods. These initial rates were then plotted as a function of substrate (S) concentration and the resulting curve was fit by nonlinear regression (KaleidaGraph) to the hyperbolic equation: $V = V_{max}[S]/([S] + K_m)$. Data obtained for HKD and HCD using the peptide substrates were conducted in side-by-side experiments to ensure that reaction conditions for the two HER-2 recombinant proteins would be identical.

that the kinetic parameters are similar for [Val^5]AgII (data not shown). Under our reaction conditions and assuming fully active protein preparations, HKD and HCD show similar k_{cat} values of 0.03−0.04 s^{-1} for AgII phosphorylation. However, published k_{cat} values for EGF receptor phosphorylation of this peptide have ranged from 0.0007 to 4.2 s^{-1} (*51*, *53*, *54*). Variations may likely reflect the oligomerization status/activation state of the receptor studied or other influences of the reaction system. It is important to keep in mind that the kinetic constants obtained using steady-state studies do not have an internal measure of protein active site concentration. Traditionally this type of analysis determines the specific activity of an enzyme by measuring the conversion of substrate per unit time per quantity of protein (usually μM/min/mg). In this calculation, one determines the protein concentration and *assumes* the protein is fully active. We have established that our enzyme has very similar specific activity and k_{cat} values as those reported for other receptor tyrosine kinases such as the EGF receptor. On the other hand a transient kinetic analysis allows the determination of the catalytically active protein concentration and below we describe our results with HKD and HCD.

Identification of an Optimal Peptide Substrate. In an attempt to identify tighter binding peptide substrates, a tyrosine kinase substrate peptide library was incubated with HCD and HKD under conditions in which approximately 2−5% of the peptide mixture was phosphorylated. Phosphopeptides were isolated and sequenced as described in the Materials and Methods. Table 2 summarizes the preferred amino acids found at each degenerate peptide position by HKD and HCD. Although limited availability of the peptide library precluded performing this experiment multiple times, the similarity of the sequences identified for each HER-2 recombinant protein tested substantiates the findings presented in Table 2.

On the basis of these results, the HER2Peptide (GGMEDIYFEFMGGKKK) was then synthesized. The alanine residues in the original peptide library were replaced with glycine residues as spacers, and the lysine residues were maintained from sequences in the library peptide to promote solubility. Steady-state reactions included 5 μM HKD or HCD, 50 μM [γ-^{32}P]ATP, and 80−2500 μM HER2Peptide, and were conducted as described above. Initial rates were measured and plotted against peptide concentration for determination of K_m and V_{max}, and results are summarized in Table 1.

Substrate Dependence on C-Terminal Lysines: Conversion to Inhibitory Peptides. While residues more than ∼5 amino acids distal to the phosphorylated tyrosine are often felt to have a minimal influence on the ability of a given peptide to serve as a kinase substrate, this thought has not been directly tested to our knowledge. In our peptide library, three C-terminal lysines were included to promote peptide solubility, and these were maintained in the HER2Peptide. Through serendipity, however, a truncated HER2Peptide lacking the terminal three lysines was synthesized to yield the peptide GGMEDIYFEFMGG (HER2−13mer). This abbreviated peptide was tested for its ability to serve as a substrate in the HER-2 kinase assay. Contrary to our expectation, phosphorylation of this truncated sequence was not observed. Moreover, we noted a dose-dependent decrease in HER-2 autophosphorylation in the presence of this peptide indicating inhibitory activity (data not shown). To determine whether this loss of substrate activity was unique to the HER2Peptide, two other lysine-truncated forms of alternate optimal substrates for HER-2 obtained from the peptide library screen—HKD-13mer (GGMEDIYFGFMGG) and HCD-13mer (GGMEDIYFHFMGG)—were subsequently synthesized and tested for their ability to serve as either HER-2 substrates or inhibitors. Like the shortened HER2−13mer peptide, these peptides were unable to serve as substrates for HER-2 and were able to inhibit autophosphorylation (data not shown). Steady-state inhibition assays were conducted as described in the Materials and Methods to further characterize the ability of these truncated sequences to serve as kinase inhibitors. A preliminary assessment of the HCD-13mer to act as a competitive inhibitor of peptide substrate binding suggests that this peptide has a K_i in the range of 40−60 μM. Similar preliminary experiments with truncated HER2−13mer (K_i = 20−40 μM) and HKD-13mer showed similar competitive inhibitory activity (data not shown).

Reversibility of HER-2 Autophosphorylation. Examination of time courses for catalysis by HKD and HCD suggested that reactions containing limiting amounts of ATP do not completely turnover this nucleotide substrate. Instead, the reaction appears to expend only 60 to 80% of the initial ATP present, as determined by SDS−PAGE/phosphor-imager analysis of reaction products (data not shown). To address whether this failure for the reaction to proceed to completion may be due at least in part to its reversibility, we assessed the ability of pre-phosphorylated HKD and HCD to undergo dephosphorylation. Enzymes were self-phosphorylated using [γ-^{32}P]ATP to a maximum stoichiometry of ∼1.3 μM $^{32}P_i$ and ∼3.8 μM $^{32}P_i$ per μM HKD and HCD, respectively, and excess nucleotides removed by biospin chromatography as described in the Materials and Methods. Although HKD theoretically retains only one of the known autophosphorylation sites of HER-2, it is possible that our observation of 1.3 μM P_i/μM enzyme may be due to inaccuracies in protein concentration assessments (determined by Bio-Rad protein assay using BSA as standard) or to revelation of cryptic autophosphorylation sites secondary to C-terminal truncation (*55*). For dephosphorylation studies, ^{32}P-HKD and ^{32}P-HCD

Table 2: Substrate Specificities of HKD, HCD and the EGF Receptor (EGFR)[a]

	peptide position relative to tyrosine								
	−4	−3	−2	−1	0	+1	+2	+3	+4
HKD	M(3.2) R(2.4)	E(2.6)	D(2.0) E(2.0)	E(2.3) D(2.1) A(1.5)	Y	F(1.9) D(1.6) E(1.6) I(1.5)	F(1.7) G(1.6) M(1.5)	F(2.1) L(1.4)	F(2.2) M(1.6) G(1.6)
HCD	M(1.9) R(1.6)	E(1.7)	D(1.6)	I(2.0) N(1.6)	Y	F(3.2) V(2.8) I(2.4) M(1.7) L(1.7)	F(1.9) H(1.8) M(1.6)	F(3.2) L(2.3) I(1.9) M(1.7) V(1.6)	F(2.3) M(1.8)
EGFR	E(1.6) D(1.5) R(1.5)	E(2.9) D(1.8)	E(2.6) D(1.5)	E(2.5) D(2.1) I(1.6)	Y	F(2.1) V(1.9) I(1.7) E(1.5)	E(1.9) F(1.6) D(1.5)	L(1.7) I(1.7) F(1.6) V(1.5)	V(1.6)

[a] A peptide substrate library with sequence Met-Ala-X-X-X-X-Tyr-X-X-X-X-Ala-Lys-Lys-Lys (where X indicates all amino acids except tryptophan, cysteine, tyrosine, serine, or threonine) was screened with HKD and HCD as described in the Materials and Methods or with EGFR as reported by Songyang et al. (*47*). Values in parentheses indicate relative selectivities of the proteins for the amino acids at the noted position. In this system, amino acids with values greater 1 are selected by the kinase; those less than 1 are selected against. Only amino acids with selectivity factors ≥1.5 are shown.

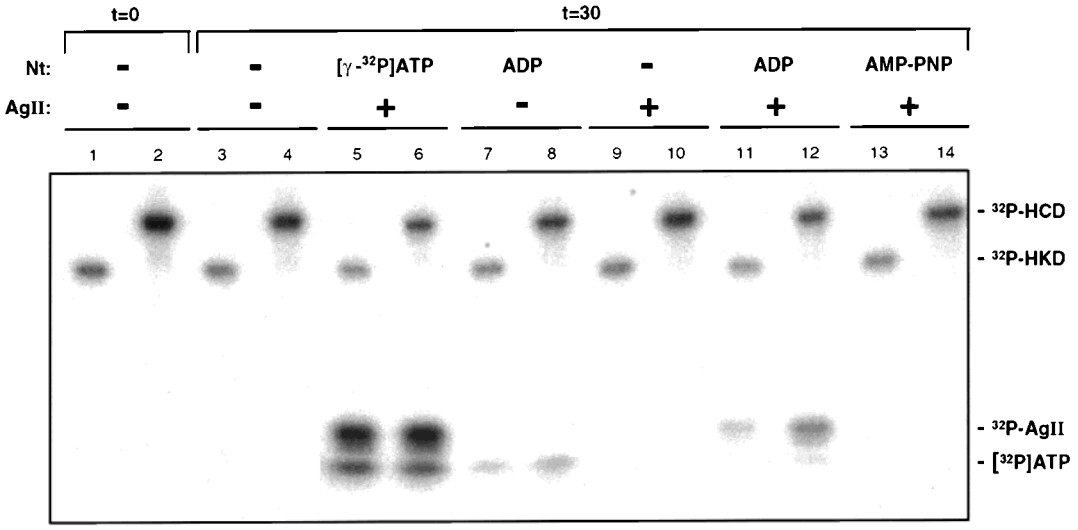

FIGURE 2: Probing for a phospho-enzyme intermediate. ^{32}P-labeled, self-phosphorylated HCD and HKD were generated as described in the Materials and Methods. After removal of excess [γ-^{32}P]ATP (lanes 1 and 2), the ^{32}P-labeled enzymes were then incubated for 30 min (lanes 3−14) in the presence or absence of 5 mM [Val^5]AgII and/or 100 μM of the indicated nucleotide, as noted above each lane (lanes 3−14).

at a concentration of 3 μM were incubated for various times at 25 °C with 10 mM $MnCl_2$ and 20 μM ADP. Incubation of ADP with pre-phosphorylated recombinant HER-2 proteins resulted in the time-dependent formation of a low-molecular weight radioactive band apparent by SDS−PAGE/phospho-imager analysis. Formation of this newly generated radioactive species was dependent upon the presence of ADP, and the radioactive species coeluted with ATP when analyzed on PEI-cellulose thin-layer chromatography plates (data not shown).

Alternative Nucleotide Substrates. The ability of self-phosphorylated HCD to phosphorylate other nucleotide-diphosphates was examined using 100 μM GDP, CDP or UDP in the presence of 10 mM $MnCl_2$ or $MgCl_2$. These studies demonstrated that GDP but not CDP or UDP can reverse the autophosphorylation reaction (data not shown). Hence, a comparison of the utilization of GTP or ATP as the nucleotide phosphate donor for the HCD autophosphorylation reaction was then conducted. Using 5 μM HCD and 100 μM [γ-^{32}P]ATP (0.5 mCi/mmol) or 100 μM [γ-^{32}P]GTP (0.5 mCi/mmol), the rate of HCD autophosphorylation catalyzed by ATP was 0.26 ± 0.03 μM s^{-1} and that catalyzed by GTP was 0.48 ± 0.10 μM s^{-1}.

Probing the Existence of a Phosphoenzyme Intermediate. Previous studies with cAPK have used a stereochemical analysis of chiral ATP to examine whether a phosphoenzyme intermediate is involved in phosphoryl transfer (*56*). Here we describe a more direct approach to explore the potential existence of a phospho-enzyme intermediate by examining the ability of pre-phosphorylated recombinant HER-2 proteins to phosphorylate an exogenous peptide substrate without additional ATP. First, HKD or HCD was self-phosphorylated and excess nucleotide removed as described above (Figure 2, lanes 1 and 2). The preservation of enzymatic activity after the self-phosphorylation procedure was confirmed by the ability of the labeled proteins to phosphorylate [Val^5]-AgII upon addition of [γ-^{32}P]ATP (Figure 2, lanes 5−6). That the self-phosphorylation reaction is reversible was again demonstrated by the generation of [γ-^{32}P]ATP after addition of ADP (Figure 2, lanes 7−8), and the dependence of this

formation on the presence of ADP argued against the presence of a contaminating phosphatase in our enzyme preparations (Figure 2, lanes 3−4 vs lanes 7−8).

Should HER-2 phosphorylate exogenous substrates through the formation of a phosphoenzyme intermediate and if that intermediate could be created and accumulated with the addition of ATP during the self-phosphorylation reaction, then the mere addition of a peptide substrate such as AgII to the isolated phosphoenzyme intermediate should result in the formation of phosphorylated peptide. However, no radioactive ^{32}P-[Val^5]AgII could be detected when this peptide substrate was added to the self-phosphorylated enzymes (Figure 2, lanes 9 and 10). It is only with the addition of ADP that formation of radioactive ^{32}P-[Val^5]AgII occurs (Figure 2, lanes 11 and 12), suggesting that the reaction had to first proceed in the reverse direction to form [γ-^{32}P]ATP, which could then be used to form the radioactive peptide. Indeed, a small amount of [γ-^{32}P]ATP is also detected in these lanes (Figure 2, lanes 11 and 12). Figure 2, lanes 13 and 14, demonstrates that the self-phosphorylated enzyme cannot phosphorylate [Val^5]AgII even in the presence of AMP-PNP, reducing the possibility that a phosphoenzyme intermediate might exist but require the presence of a bound nucleotide for activity.

Steady-State Kinetics of Nucleotide Binding. *N*-Methylanthraniloyl (mant) derivatives have been successfully employed to probe the kinetics of nucleotide binding to proteins (*43*). Among the advantages that the mant derivatives provide is their sensitivity to hydrophobic microenvironments, which generally translates to a two- to 3-fold enhancement of their fluorescence intensities on protein binding (*43*, *44*). Moreover, their long emission maxima (∼445 nm) allows for little or no interference from the intrinsic fluorescence of tyrosine and tryptophan residues (∼340 nm) (*43*). Quite conveniently, mant-nucleotides have an excitation maximum (∼350 nm) near the emission maximum of tryptophan and tyrosine, thereby enabling the specific excitation of only protein-bound nucleotides through fluorescence energy transfer when these aromatic amino acids are excited at ∼280 nm (*43*). Thus, mant-nucleotides provide a sensitive and specific probe for analyzing protein−nucleotide interactions.

In an effort to characterize the binding of ATP with the HER-2 recombinant proteins, this step was isolated using the non-hydrolyzable ATP analogue, AMP-PNP. AMP-PNP has been shown to be a potent inhibitor of EGF receptor autophosphorylation, with a K_i approximately equal to the K_m of ATP (*57*). Thus, this nucleotide was derivatized to form the fluorescent analogue mantAMP-PNP for examination of nucleotide binding to HER-2. Furthermore, mantADP was also made for the detection of events involved in product release. To determine the influence of the mant group on nucleotide binding to the HKD and HCD recombinant proteins, the ability of AMP-PNP, mantAMP-PNP, ADP, and mantADP to compete with ATP in autophosphorylation experiments was examined. The inhibition constants were measured as noted in the Materials and Methods. Results of these studies are summarized in Table 3.

Table 3: Steady-State Kinetic Parameters for HER-2 Autophosphorylation[a]

HER-2 domain	nucleotide	K_m[b] or K_i[c] (μM)	V_{max} (μM s^{-1})
HKD	ATP[b]	2.7 ± 0.4	0.14 ± 0.01
	AMP-PNP[c]	26 ± 6	0.12 ± 0.00
	mantAMP-PNP[c]	30 ± 6	0.15 ± 0.01
	ADP[c]	3.1 ± 0.2	0.15 ± 0.01
	MantADP[c]	6.5 ± 1.8	0.16 ± 0.02
HCD	ATP[b]	8.8 ± 1.2	0.31 ± 0.01
	AMP-PNP[c]	23 ± 4	0.37 ± 0.00
	mantAMP-PNP[c]	25 ± 1	0.36 ± 0.01
	ADP[c]	11 ± 3	0.34 ± 0.01
	mantADP[c]	11 ± 1	0.41 ± 0.04

[a] 5 μM enzyme was included each experiment. [b] K_m and V_{max} for ATP were determined for autophosphorylation of HER-2 recombinant proteins as described in Table 1. [c] K_i and V_{max} for the other nucleotides were determined in competition experiments with ATP for their ability to inhibit enzyme autophosphorylation, as described in the Materials and Methods.

Nucleotide Binding to HER-2. Stopped-flow fluorescence spectroscopy was used to analyze the events associated with nucleotide binding to HKD and HCD. Measurements were performed under pseudo-first-order reaction conditions ([mant-nucleotide] ≥ 10 times [enzyme]). Protein binding to mantAMP-PNP or mantADP results in an increase of fluorescence as detected at 450 nm (Figure 3A). That the observed fluorescence signals were due to interactions between the mant-nucleotide and the HER-2 recombinant proteins was independently confirmed through the lack of fluorescence changes in the absence of these enzymes as well as in the presence of nonnucleotide binding protein 3-deoxy-D-manno-2-octulosonate-8-phosphate (Kdo8P) synthase (data not shown). The time-dependent changes in fluorescence observed at each nucleotide (Nt) concentration were fit to a single exponential to determine the observed rate constant (k_{obs}) for each transient, and the resulting data were fit according to the following one-step binding mechanism:

$$E + Nt \underset{k_{-1}}{\overset{k_1}{\rightleftharpoons}} E{\cdot}Nt$$

thus

$$k_{obs} = k_1[Nt] + k_{-1}$$

Accordingly, the association and dissociation rate constants, k_1 and k_{-1}, could then be determined respectively from the slope and y-intercept of curves obtained by plotting k_{obs} as a function of the concentration of the mant-nucleotide (Table 4). These studies were conducted for HKD and HCD in both the unphosphorylated and pre-phosphorylated states. At all concentrations of nucleotide employed (7.5−120 μM), k_{obs} displayed a linear dependence on substrate concentration upon interaction of HCD with mantAMP-PNP (Figure 3B). Additional mantAMP-PNP concentrations (up to 480 μM) in studies of HKD also revealed a continued linear dependency of rate on nucleotide concentration at these higher concentrations as well (Figure 3C). Further increases in nucleotide were not possible under our assay conditions, as a precipitate became evident at mant-nucleotide concentrations of ≥1 mM.

Nucleotide Dissociation Competition Experiments. The dissociation rate constants for mantAMP-PNP and mantADP were measured directly by competition with an excess of a competing nucleotide. In these experiments, the HER-2 recombinant enzyme (2−2.5 μM) was preincubated with

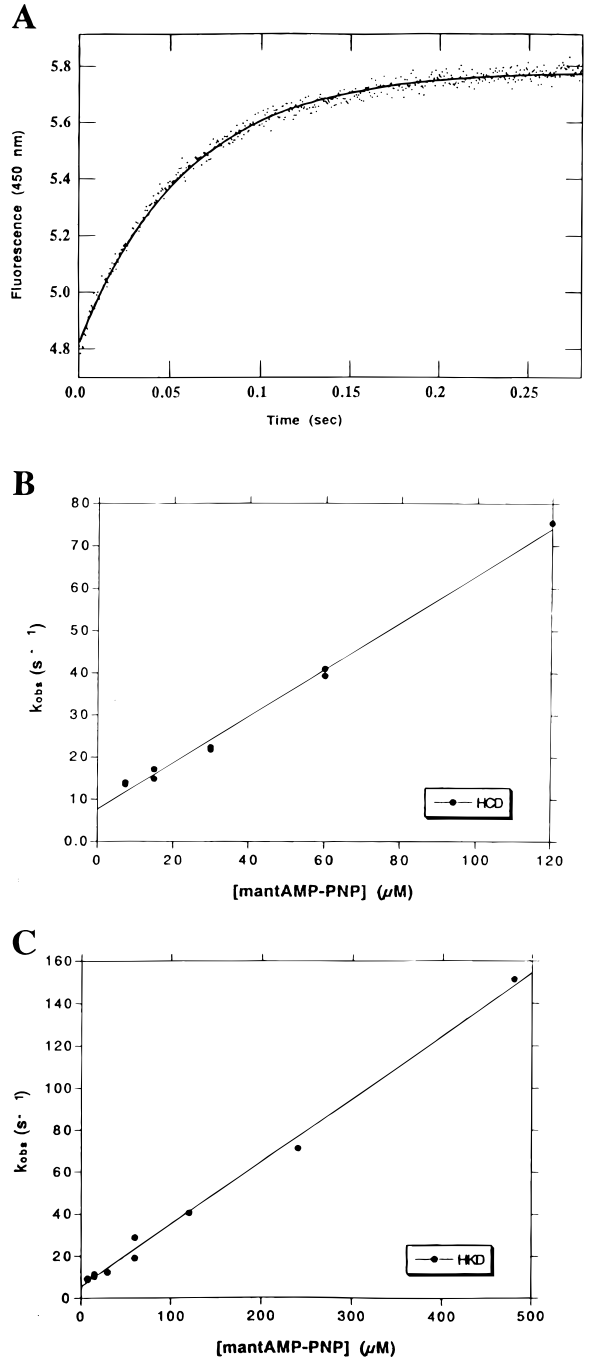

FIGURE 3: (A) Representative stopped-flow fluorescence trace measuring the apparent binding rate of nucleotide to HCD using fluorescence energy transfer. A reaction mixture containing 0.75 μM HCD and 15 μM mantAMP-PNP was excited at 290 nm, and fluorescence was detected using a 450 nm interference filter. The average of four traces is shown. Fitting the data to a single-exponential equation ($F = A \exp(-k_{obs}t) + C$) resulted in an observed rate constant (k_{obs}) of 17.1 s^{-1}. Determination of the association rate constant for mantAMP−PNP to (B) HCD and (C) HKD. (B) The fluorescence signals detected by stopped-flow fluorescence spectroscopy using 0.75 μM HCD and 7.5−120 μM mantAMP-PNP were fit to single-exponential equations to determine the observed rate constant (k_{obs}) at each mantAMP-PNP concentration used. These values were then plotted as shown and the data fit to a line ($k_{obs} = k_{on}$[mantAMP-PNP] + k_{off}) by nonlinear regression using KaleidaGraph. The resulting slope is equivalent to the association rate constant (k_{on}), while the y-intercept provides a measure for the dissociation rate constant (k_{off}). (C) 0.75 μM HKD was examined for its interactions with 7.5−480 μM mantAMP-PNP by similar methods.

Table 4: Summary of Rate Constants Determined by Stopped-Flow Fluorescence Experiments

HER-2 domain	nucleotide	k_{on}[a] (μM^{-1} s^{-1})	k_{off}[a] (s^{-1})	k_{off}[b] (s^{-1})	K_d[c] (μM)
HKD	mantAMP-PNP	0.30 ± 0.01	3.6 ± 1.6	5.1 ± 0.5	17 ± 2
	MantADP	0.23 ± 0.04	2.9 ± 1.3	2.0 ± 0.0	8.6 ± 1.4
	MantATP	0.23 ± 0.01	5.5 ± 0.4	N/A	24 ± 2[a]
P−HKD	mantAMP-PNP	0.54 ± 0.04	9.0 ± 2.2	9.6 ± 0.3	18 ± 1
	MantADP	0.27 ± 0.03	5.7 ± 1.1	3.6 ± 0.5	13 ± 2
HCD	mantAMP-PNP	0.56 ± 0.02	6.9 ± 1.5	12 ± 0	21 ± 1
	MantADP	0.30 ± 0.01	4.3 ± 0.5	3.8 ± 0.4	13 ± 1
P−HCD	mantAMP-PNP	0.34 ± 0.02	17 ± 1	19 ± 0	55 ± 4
	MantADP	0.26 ± 0.00	7.9 ± 0.2	7.2 ± 0.1	28 ± 0

[a] Nucleotide binding experiments were conducted at each of four or five nucleotide concentrations covering the ranges indicated in the text. The dissociation rate constants from nucleotide binding experiments (k_{off}) were determined as described in the text. [b] Direct measurements of the dissociation rate constant (k_{off}) from competition experiments. On average, three separate determinations were performed for each enzyme-nucleotide pair. [c] Unless otherwise indicated, K_d was determined from the ratio of k_{off}/k_{on}.

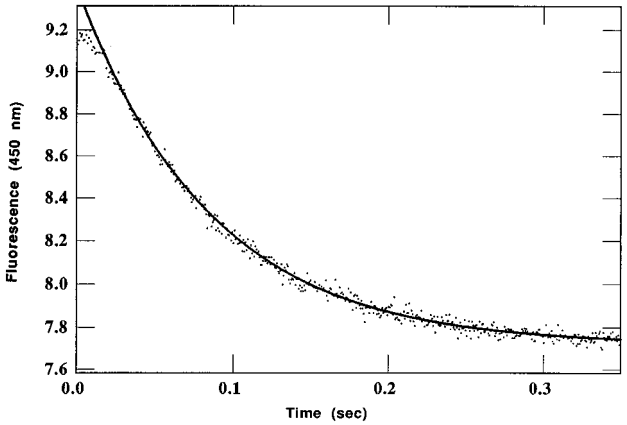

FIGURE 4: Representative stopped-flow fluorescence trace measuring the dissociation rate for nucleotide from HCD using fluorescence energy transfer. 2 μM HCD was preincubated with 10 μM mantAMP-PNP. The dissociation of this complex was then induced by mixing with 500 μM AMP-PNP, and the resulting decrease in fluorescence at 450 nm was monitored over time. A fit to a single-exponential equation ($F = A \exp(-k_{obs}t) + C$) results in a dissociation rate constant (k_{obs}) of 12.0 s^{-1}.

stoichiometric amounts (10 μM) of mantAMP-PNP or mantADP in one syringe of the stopped-flow apparatus. This solution was then rapidly mixed with a solution containing an excess (0.5−1 mM) of ATP or AMP-PNP in the other syringe. The resulting displacement of the protein-bound mant-nucleotide from the HER-2 enzymes causes a decrease in fluorescence at 450 nm which can be monitored over time. For these studies, 10 μM mantAMP-PNP was included in the second syringe as well as the first in order to avoid artifactual dissociation of the mant fluorophore from the HER-2 enzymes induced by dilutional effects. Fitting these fluorescence changes to a single-exponential decay expression provides the dissociation rate constant (k_{off}) for the mant-nucleotide. A representative fluorescence transient for the release of mantAMP-PNP from HCD is depicted in Figure 4. Competition experiments were conducted for HKD and HCD in both the pre-phosphorylated and unphosphorylated states, and the results are summarized in Table 4. On average, three separate determinations were performed for each mant-nucleotide. For each enzyme·mant-nucleotide pair, similar dissociation rate constants were obtained regardless of the

Table 5: Summary of Kinetic Parameters Determined by Rapid Chemical Quench Analysis[a]

HER-2 domain	amplitude (μM)	k_b (s^{-1})	V_{ss} ($\mu M\ s^{-1}$)	$k_{ss} = V_{ss}/A$ (s^{-1})
HKD	1.1 ± 0.2	3.5 ± 1.0	1.6 ± 0.1	1.4 ± 0.2
HCD	1.0 ± 0.2	3.9 ± 1.0	1.0 ± 0.2	0.93 ± 0.32
P−HKD	0.69 ± 0.14	3.2 ± 0.3	2.1 ± 0.0	3.0 ± 0.6

[a] 10 μM enzyme was used in these experiments.

identity of the competing nucleotide used. It should be noted that this direct method for measuring k_{off} is more accurate than approximations obtained from linear extrapolations in the nucleotide association studies reported in the previous section. Hence, K_d values reported in Table 4 were determined using the more accurate k_{off} values from these nucleotide dissociation competition experiments.

Examination of Chemical Catalysis through Rapid Chemical Quench Measurements. The first step in defining the reaction kinetics and examining chemical catalysis for peptide phosphorylation was to conduct a pre-steady-state burst experiment to identify the rate-limiting step in the overall reaction pathway. In this type of experiment, the peptide is used in slight excess over enzyme such that the first enzyme turnover as well as multiple turnovers can be examined. We used the HER2Peptide and rapid chemical quench experiments to examine the phosphorylation of peptide by HCD and HKD enzymes. Having determined the K_m of HER2Peptide to be ~350 μM (Table 1), we used this peptide at a minimum concentration of 2000 μM in rapid chemical quench reactions with HKD and HCD to define the reaction kinetics. Higher concentrations of this peptide could not be achieved in our experiments without inducing significant precipitation in the reaction mixture. The time-dependent formation of radiolabeled HER2Peptide for pre-steady-state burst experiments using HCD and HKD are shown in Figure 5, panels A and B. Examination of these curves demonstrated that formation of phosphopeptide occurs in a biphasic manner, with an initial exponential phase followed by a slower linear phase. Hence, these time courses were fit to an equation describing a pre-steady-state burst (see Materials and Methods) and the kinetic parameters are summarized in Table 5. Under these conditions, an amplitude corresponding to approximately 10% active enzyme sites was observed.

A pre-steady-state burst experiment was also performed using self-phosphorylated HKD in order to observe the effects of autophosphorylation on chemical catalysis (Figure 6, Table 5). The similarities in the magnitudes of the resulting exponential burst (k_b) and steady-state rate (V_{ss}) makes discrimination of the two phases less evident. However, the curvature in the data can be more easily appreciated when linear curve fits are attempted (Figure 6, inset). Difficulties in preparing prephosphorylated HCD at the required concentrations precluded our ability to conduct similar studies on HCD.

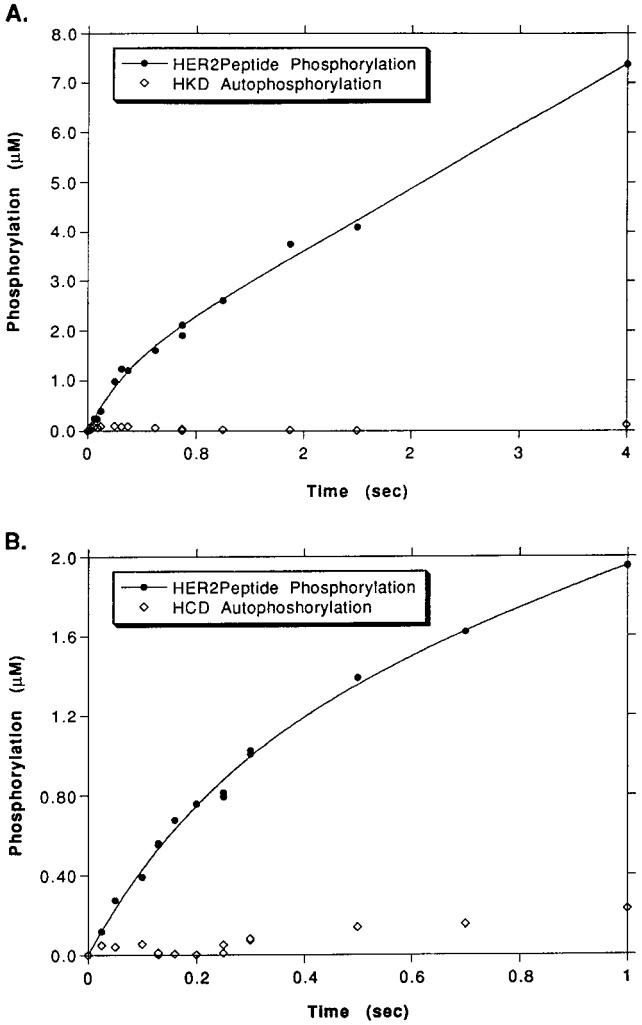

FIGURE 5: Phosphorylation of HER2Peptide under pre-steady-state burst conditions using (A) HKD or (B) HCD. Reactions were conducted using 10 μM enzyme, 2000 μM HER2Peptide, and 100 μM [γ-^{32}P]ATP (0.5 mCi/mmol). Data for HER2Peptide phosphorylation (filled circles) were fit to a burst equation (Materials and Methods). Also shown is the amount of concomitant autophosphorylation events (open diamonds).

DISCUSSION

Given the central role that the HER-2 tyrosine kinase plays in effecting the receptor's biological and pathological processes, an understanding of its catalytic mechanism is fundamental for discerning the mechanistic implications of the action of inhibitors, effects of autophosphorylation and consequences of protein interactions. Hence, we have conducted steady-state and pre-steady-state characterizations of phosphorylation reactions catalyzed by the HER-2 tyrosine kinase using protein purified to homogeneity from a baculovirus expression system. The transient kinetic analysis has allowed us to construct a minimal kinetic scheme that defines the kinetic reaction pathway. We describe the studies that lead to the kinetic pathway for HER-2 tyrosine kinase and highlight similarities and differences with the serine/threonine kinase, cAPK, the only other protein kinase for which a comprehensive kinetic reaction pathway is available.

Identification of an Optimal Peptide Substrate. To determine whether the 230 amino acid tail may affect substrate specificity at the kinase active site, the selectivities of HCD and HKD for amino acids in locations flanking the peptide tyrosine were examined. Moreover, identification of a substrate with higher affinity than AgII was needed to facilitate pre-steady-state studies directed at examining the HER-2 catalyzed phosphorylation of an exogenous peptide substrate. Use of a degenerate tyrosine kinase peptide substrate library has been successful in the identification of

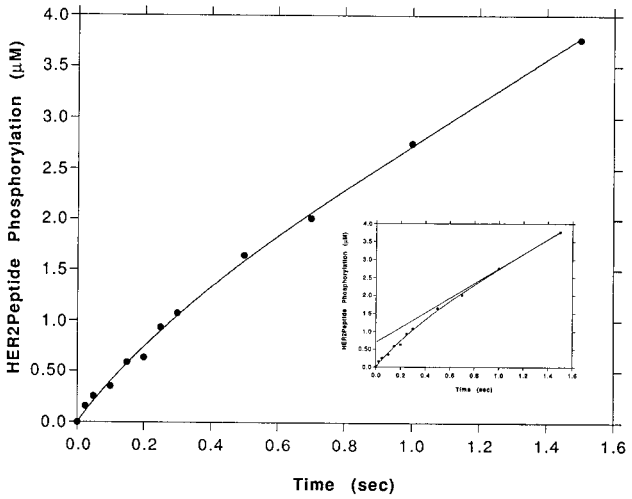

FIGURE 6: Phosphorylation of HER2Peptide under pre-steady-state burst conditions using prephosphorylated HKD. Reactions were conducted using 9.9 μM enzyme, 2000 μM HER2Peptide, and 100 μM [γ-^{32}P]ATP (0.5 mCi/mmol). Data were fit to a burst equation (Materials and Methods). (Inset) The linear phase is extrapolated to the *y*-axis.

optimal sequences for several kinases (*46*, *47*). For instance, this technique determined the substrate preference of the insulin receptor to be XEEEYMMMM, which is strikingly similar to the YMNM sequence found in this receptor's in vivo substrate insulin receptor substrate-1 (IRS-1) (*47*). Furthermore, synthesis of a peptide based on the sequence identified for src kinase produced a peptide with $K_m = 33$ μM for this enzyme (*47*). Hence, both HER-2 recombinant proteins were screened for optimal peptide substrates using this method.

Results from this screen for both HCD and HKD (Table 2) indicate that like other receptor tyrosine kinases previously studied, the HER-2 recombinant proteins have an affinity for a large hydrophobic residue three amino acids downstream from the phosphorylatable tyrosine (*47*). In addition, phenylalanine residues are highly preferred in positions C-terminal to the tyrosine, as is the case for the EGF receptor (*47*). Incidentally, the crystal structure of the insulin receptor core tyrosine kinase domain in the phosphorylated, activated state determined in the presence of an IRS-1-derived peptide substrate (KKKLPATGDYMNMSPVGD) shows that the peptide methionines one and three residues downstream from the phosphorylatable tyrosine interact with hydrophobic pockets of the kinase (*58*). Likewise, a comparable role may be postulated for the residues of HER-2 peptide substrates C-terminal to the tyrosine.

Synthesis of a peptide (HER2Peptide) with the sequence GGMEDIYFEFMGGKKK resulted in a substrate of K_m ~350 mM for both HER-2 recombinant proteins. On the basis of k_{cat}/K_m, the recombinant HER-2 proteins have specificities approximately 10-fold stronger for HER2Peptide than for AgII. Thus, the HER-2 recombinant proteins have a selectivity similar to that of the EGF receptor, and the additional 230 amino acids of HCD do not appear to alter the selectivity of the core kinase domain for peptide substrates.

Substrate Dependence on C-Terminal Lysines: Conversion to Inhibitory Peptides. Protein kinase-substrate interactions are thought to depend on the primary sequence immediately flanking the phosphorylated tyrosine and not extensively on more distal residues (*47*). On the basis of such observations, some degenerate peptide libraries have been constructed with terminal regions believed to be passive in the library's substrate behavior. While specificity may be derived from the degenerate portion of the peptide sequence, the constant terminal regions may have an influence on substrate activity as well. In the case of the HER2Peptide, removal of the terminal 3 lysine residues resulted in a competitive inhibitor for this substrate. Therefore, caution should be observed when attempting to extrapolate the result of degenerate library screening to the identification of protein kinase substrates based solely on the degenerate region of the library.

Steady-State Characterization of Nucleotide Binding. To determine how well the HER-2 recombinant proteins tolerate the additional *N*-methylanthraniloyl moiety of the mant derivatives, these analogues were compared with their parent nucleotides in terms of their ability to inhibit autophosphorylation reactions containing ATP. Lineweaver−Burke analyses in the presence and absence of the various analogues demonstrate that these nucleotides are competitive with ATP (data not shown). Moreover, comparing the K_i values for mantAMP-PNP vs AMP-PNP and mantADP vs ADP indicate that the *N*-methylanthraniloyl moiety has little effect on the ability of the parent nucleotide to compete with ATP (Table 3). Hence, mant-derivatives closely mimic their parent nucleotides in binding HER-2, and can therefore be used for studying these interactions.

These data indicate that the HER-2 tyrosine kinase binds nucleotides with reasonably high affinity. Indeed, the K_i of the product ADP is approximately that of the K_m for ATP. Thus, although the mechanism for exogenous substrate phosphorylation by the EGF receptor is formally random (*59*), this high affinity of ADP taken together with the relatively low affinity of peptide substrates suggests that the preferred pathway for HER-2 may be one involving the slower release of ADP relative to that of phosphorylated peptide product. It should be noted that while these studies are conducted in the absence of an exogenous peptide substrate, nucleotide binding to HER-2 in the presence of peptides is likely to be similar, since the K_m for ATP determined in the presence or absence of peptides yields comparable values.

Stopped-Flow Transient Kinetic Analysis of Nucleotide Binding. In these studies, the unique excitation and emission spectra of aromatic amino acids in HER-2 and that of mant-nucleotides was exploited to specifically report on the presence of bound nucleotides in the HER-2 active site through fluorescence energy transfer. Hence, the observed fluorescence transients for these nucleotides specifically reflect their association with and dissociation from the HER-2 proteins. Since the measured events are thus simple first-order processes, the corresponding rate constants are independent of the concentration of enzyme active sites.

The K_i values for each nucleotide determined under steady-state conditions are similar to the K_d values obtained using stopped-flow methodologies (Tables 3 and 4). However, the latter method provides the basis for differences in nucleotide affinities. In particular, whereas the association rate constants are fairly similar for all nucleotides studied, the dissociation rate constants vary significantly among the various nucle-

otide−protein complexes and, thus, ultimately contribute more to differences among K_d values than the association rate constants (Table 4). Hence, these results suggest that ATP itself probably also has an association rate constant comparable to those measured in Table 4. Indeed, stopped-flow measurements of HKD using the hydrolyzable mant-ATP compound yielded an association rate constant of 0.23 μM^{-1} s^{-1}, which is very similar to those of the other nucleotides (Table 4). Significantly, the data in Table 4 shows that the larger HCD protein releases nucleotides approximately 2-fold faster than the HKD protein. Hence, these observations suggest that the additional 230 amino acids in the HCD carboxyl terminus affects nucleotide affinity by facilitating their release. For these studies, the kinetics of nucleotide binding to HKD and HCD in both the nonphosphorylated and pre-phosphorylated forms was examined. Again, while there is little variability among the association rate constants, the dissociation rate constants provide the major source of differences in relative nucleotide affinities for these enzyme states. Interestingly, pre-phosphorylation of both HER-2 recombinant proteins is associated with an approximately 2-fold increase in the dissociation rate constants relative to the nonphosphorylated enzymes for all nucleotides tested (Table 4), suggesting that phosphorylation of HER-2 facilitates nucleotide release.

Examination of Chemical Catalysis Using Rapid Chemical Quench Measurements. To examine the steps after substrate binding, rapid chemical quench pre-steady-state burst experiments were performed using HER2Peptide. The rapid chemical quench data reveal the existence of an initial burst phase followed by a slower linear phase of phosphopeptide formation. This biphasic nature of product formation corresponds to the existence of at least two steps following substrate binding for both HER-2 recombinant proteins. In terms of enzyme specific activity, the steady-state V_{max} values for HER2Peptide phosphorylation (Table 1) is in good agreement with the V_{ss} values obtained from the linear phase of these pre-steady-state experiments. In these studies, the HER-2 recombinant proteins (E) were preincubated with the HER2Peptide substrate (S) before mixing with an excess of ATP (≥10-fold K_m). Hence, a model consistent with these observations is as follows:

Scheme 2

$$E{\cdot}S + ATP \underset{k_{-1}}{\overset{k_1}{\rightleftharpoons}} E{\cdot}ATP{\cdot}S \underset{k_{-2}}{\overset{k_2}{\rightleftharpoons}} E{\cdot}P{\cdot}ADP \underset{k_{-3}}{\overset{k_3}{\rightleftharpoons}} E + ADP + P$$

where the binding of ATP occurs in a rapid equilibrium, step two (chemical catalysis) is defined by the exponential burst phase, and step three (event after chemistry) is described by the linear phase of the pre-steady-state experiments. While step three is a simplified step representing a rate-limiting event that occurs after chemistry, the release of the phosphopeptide is unlikely to be rate-limiting because of the weak affinity of the unphosphorylated peptide (0.4 mM). Given the time frame of the reaction course (within 4 s) and the large excess of reactants used, the reverse reaction is not likely to be significant under the pre-steady-state burst conditions, and the measured k_b and V_{ss} values in these experiments thereby more closely reflect the forward components for steps two (k_2) and three (k_3), respectively.

As shown in Table 5, the burst amplitudes for the unphosphorylated HKD and HCD proteins are only about 10% of the enzyme concentration, as determined by Bio-Rad protein assay. The failure to detect a full-amplitude burst may be governed by several factors including the presence of inactive enzyme and/or to characteristics of the reaction kinetics. Several issues need to be raised regarding the active site concentration. As indicated below, a complete analysis of the reaction kinetics indicates that the active site concentration is closer to 20%. It is important to keep in mind that a pre-steady-state burst experiment provides a measure of the concentration of sites on the enzyme that are catalytically active. With the exception of studies on cAPK (*16*), no other protein kinase has been evaluated using a pre-steady-state kinetic analysis to determine the true active site concentration. This is the only meaningful way one can determine what percentage of the protein active sites are functioning properly to carry out chemical catalysis.

The active site concentration reported for cAPK is 70−80%, but one must keep in mind that this is classic protein kinase which is easily expressed in bacteria and the first to be characterized both structurally and kinetically. Unfortunately, members of the receptor tyrosine kinases (and in particular, HER-2) are much more difficult to work with since they are membrane-bound, have a single polypeptide chain that contains both catalytic and regulatory activities, and often require a baculovirus expression system to obtain active protein. To obtain a soluble form of the HER-2, we needed to add detergent to prevent formation of protein aggregates. Moreover, pre-steady-state kinetic analysis on a variety of proteins indicate that a lower percentage of active sites is not uncommon for a protein that is difficult to express and with which to work. For example, transient kinetic analysis of HIV reverse transcriptase by our lab and others as well as others in the polymerase field have shown that it is not at all unusual to observe 50% active sites even on a more well-behaved, easily expressed protein (*60*, *61*).

Regardless, the burst amplitude (A) places a lower limit on the steady-state concentration of active enzyme in the enzyme−product species ([E·P·ADP]) (*62*). Hence, since in Scheme 2 the steady-state turnover rate is equal to $k_3[E{\cdot}P{\cdot}ADP]_{ss}$ under initial rate conditions, an upper limit of the rate constant for the rate-limiting linear phase (k_3) can be determined to a first approximation from the pre-steady-state burst parameters by the term, V_{ss}/A ($=k_{ss}$). This determination suggests that untreated (i.e., not pre-phosphorylated) HCD and HKD recombinant proteins catalyze the phosphorylation of HER2Peptide with a burst phase occurring ≥3-fold faster than the linear phase under the reaction conditions. It should be noted that the low affinity of HER2Peptide made further studies at higher peptide concentrations difficult and, thus, precluded the determination of the maximal burst rate constant (k_b). If tighter binding peptide substrates become available, future experiments may be helpful to better define this parameter. Nevertheless, these results place a lower limit on the rate of the chemical reaction and suggest that for HKD and HCD this step occurs faster than steady-state turnover.

The similarity of the k_{ss} values (Table 5) with the stopped-flow-determined dissociation rate constants for mantADP

(Table 4) suggests that the slower phase of the rapid-quench burst experiments may be limited at least in part by ADP release. However, comparison of the stopped-flow and rapid-quench data for the two recombinant proteins show that while stopped-flow measurements indicate that HCD releases nucleotides *faster* than HKD, the pre-steady-state burst experiments demonstrate that HCD and HKD phosphorylate peptides with *similar* rate-limiting rates (k_{ss}). Taken together, this difference between ADP release for the two domains yet lack of difference in the rate-limiting step identified by the rapid-quench data support the possibility that another event in addition to ADP release—such as a conformational change—may be invoked as rate-limiting, at least for the larger HCD protein. Transient kinetic evidence also exists for partially rate-determining conformational change(s) in the mechanism utilized by the serine/threonine kinase cAPK for the phosphorylation of an exogenous substrate (*17*−*19*). Moreover, the accumulating X-ray crystallography data for other protein kinases solved in various states of activation suggest that substrate phosphorylation by protein kinases is a dynamic process involving several conformational changes, any one of which could be kinetically significant [reviewed in Johnson et al. (*3*)].

At the high concentration (2 mM) of peptide used in these studies, very little self-phosphorylation occurs relative to that of exogenous peptide. Significantly, the burst amplitudes for the unphosphorylated HKD and HCD preparations are greater than the levels of self-phosphorylated enzyme that accumulate during the course of the reaction (Figure 5), suggesting that self-phosphorylation of the HER-2 tyrosine kinase is not a prerequisite for activity. These results support those of Sherril (*63*), who came to the same conclusion for the EGF receptor using an antibody-inducible system for enzyme activation. In those studies, it was observed that disruption of EGF receptor oligomers resulted in a concomitant decrease in enzymatic activity despite autophosphorylation of receptor tyrosine residues. While not necessary for catalysis, however, self-phosphorylation of the HKD protein does potentially appear to be associated with a slight enhancement of the rate-limiting step (Table 5) and, this modification does not seem to impact the actual rate of chemistry (k_2, Scheme 2) under these conditions. Moreover, the stopped-flow studies provide further evidence supporting an active role of self-phosphorylation in enzyme catalysis not otherwise detectable in the steady-state measurements of V_{max}. Prior to this, self-phosphorylation of HER-2 has only been thought to affect catalysis by eliminating competition with exogenous substrates for the active site otherwise imposed by the autophosphorylatable tyrosine residues (*48*, *64*, *65*). That self-phosphorylation actually directly affects the catalytic mechanism of HER-2 by enhancing the rates of ADP release and of the rate-limiting step has never been demonstrated.

Proposed Mechanism for Phosphoryltransfer by the HER-2 Tyrosine Kinase. On the basis of this work, the kinetic mechanism for HER-2-catalyzed tyrosine phosphorylation reactions involves substrate binding followed by chemical catalysis and product release. In addition, a rate-limiting conformational change may occur, either before or after product release. Thus, a scheme consistent with these observations is as follows:

Scheme 3

$$\mathrm{E} + \mathrm{ATP} \underset{k_{-1}}{\overset{k_1}{\rightleftharpoons}} \mathrm{E{\cdot}ATP} + \mathrm{S} \underset{k_{-2}}{\overset{k_2}{\rightleftharpoons}} \mathrm{E{\cdot}ATP{\cdot}S} \underset{k_{-3}}{\overset{k_3}{\rightleftharpoons}}$$
$$\mathrm{E{\cdot}ADP{\cdot}P} \underset{k_{-4}}{\overset{k_4{}^*}{\rightleftharpoons}} \mathrm{E'{\cdot}ADP{\cdot}P} \underset{k_{-5}}{\overset{k_5}{\rightleftharpoons}} \mathrm{E{\cdot}ADP} + \mathrm{P} \underset{k_{-6}}{\overset{k_6}{\rightleftharpoons}} \mathrm{E} + \mathrm{ADP}$$

wherein "E" represents enzyme, "S" represents an unphosphorylated tyrosine-containing substrate, "P" represents the phosphotyrosine- containing product, and the asterisk (*) indicates the likely rate-limiting step.

Although experiments addressing the order of substrate binding or that of product dissociation have not yet been performed for HKD and HCD, the reaction catalyzed by the EGF receptor has been determined using steady-state methodologies to be a random sequential one (*59*). Hence, it is feasible that the order of steps one and two (ATP and peptide binding) as well as of steps five and six (phosphopeptide and ADP release) may be interchangeable. In addition, a rate-limiting conformational change (step 4) is depicted as occurring before ADP or phosphopeptide release; however, the actual order of this step relative to the product release steps is unclear from our studies. Employment of substrate trapping methodologies may eventually establish the actual sequence of these events.

Thus far, the kinetic parameters for HER-2 catalysis have been determined by conventional methods in which time courses describing different portions of the pathway are fit to single exponentials alone or in combination with a linear phase. Hence, estimates for the steps depicted in Scheme 3 may be obtained as follows. Stopped-flow experiments provide measurements for the parameters of ATP association (step one) and ADP dissociation (step five). In addition, the exponential phase of the rapid quench pre-steady-state burst experiments place a lower limit on the step of chemistry (step 3), while the slower linear phase of these studies may describe the rate-limiting conformational change. Although transient kinetic studies have not been performed for the direct measurement of K_d for peptide binding (step two) due to its weak affinity, this value may be tentatively estimated by the K_m of the peptide because of the finding that this value is similar to the K_i of the peptide for inhibition of autophosphorylation (data not shown). By similar arguments, the release of phosphopeptide (step five) may be roughly approximated by the inverse of the K_m value. However, the weak affinity of the peptide suggests that its release in the phosphorylated state ought to be fast (and therefore, inconsequential to the kinetic mechanism) relative to ADP release and the rate-limiting step; moreover, studies with cAPK have shown that the phosphopeptide product has a lower affinity than its substrate counterpart (*16*). Values for each step are summarized in Table 6.

Using these experimental values, we now have reasonable estimates with which develop a minimal kinetic mechanism though computer simulation. In this method, a kinetic mechanism can be entered into the computer along with information reflecting substrate and enzyme concentrations. This information is then used to predict experimentally determined time courses. Since the entire mechanism is evaluated, data fitting by computer simulation requires no simplifying assumptions (*66*). The KinTekSim kinetic simulation program has been used by our laboratory and other

Table 6: Assignment of Experimentally Determined Kinetic Measurements to Steps in Scheme 3

Scheme 3 step no.	rate constant (Scheme 3)	experiment for measurement	measured values for HKD	measured values for HCD
1. ATP binding	k_1	SF[b]: k_{on} for mantAMP-PNP (Table 4)	$0.30 \pm 0.01\ \mu M^{-1}\ s^{-1}$	$0.56 \pm 0.02\ \mu M^{-1}\ s^{-1}$
	k_{-1}	SF: k_{off} for mantAMP-PNP (Table 4)	$5.1 \pm 0.5\ s^{-1}$	$12 \pm 0\ s^{-1}$
2. peptide binding	$k_{-2}/k_2 \approx K_m$	steady-state K_m of HER2Peptide (Table 1)	$390 \pm 110\ \mu M$	$350 \pm 30\ \mu M$
3. chemical catalysis[a]	k_3	RQ[b]: exponential burst (k_b) (Table 5)	$3.5 \pm 1.0\ s^{-1}$	$3.9 \pm 1.0\ s^{-1}$
4. conformational change[a]	k_4	RQ: linear phase (k_{ss}) (Table 5)	$1.4 \pm 0.2\ s^{-1}$	$0.93 \pm 0.32\ s^{-1}$
5. phosphopeptide release	$k_5/k_{-5} \geq K_m$	steady-state K_m of HER2Peptide (Table 1)	$390 \pm 110\ \mu M$	$350 \pm 30\ \mu M$
6. ADP release	k_6	SF: k_{off} for mantADP (Table 4)	$2.0 \pm 0.0\ s^{-1}$	$3.8 \pm 0.4\ s^{-1}$
	k_{-6}	SF: k_{on} for mantADP (Table 4)	$0.23 \pm 0.04\ \mu M^{-1}\ s^{-1}$	$0.30 \pm 0.01\ \mu M^{-1}\ s^{-1}$

[a] Since the rapid chemical quench pre-steady-state burst experiments were performed using vast excesses of substrates over very short time periods such that very little product formation occurred, the measured values more closely represent those of the forward processes. If significant reverse components exist, then the measured rate constants would represent composite values for both directions. [b] SF, stopped-flow; RQ, rapid quench.

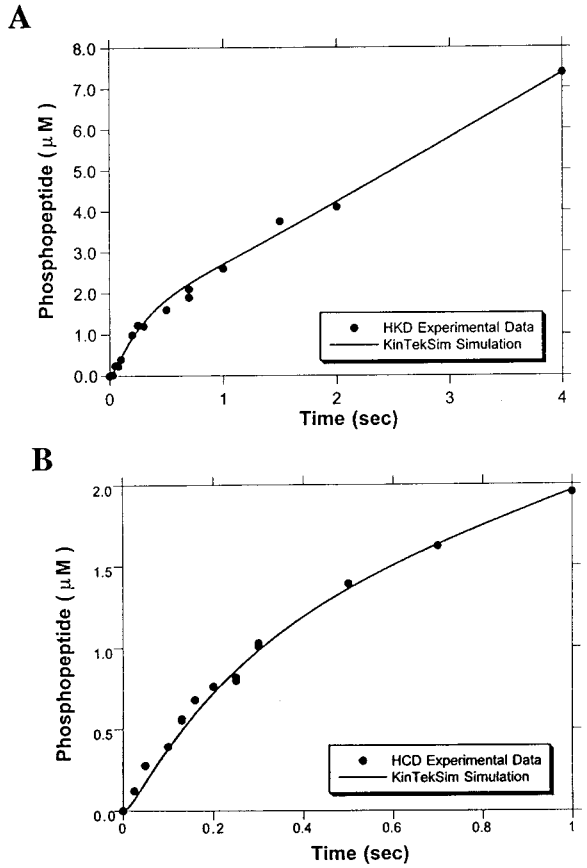

FIGURE 7: Simulation of HER2Peptide phosphorylation under pre-steady-state burst conditions for (A) HKD and (B) HCD. The kinetic mechanism described by Scheme 3 and the values in Table 6 were used to generate the curves in both panels with the KinTekSim computer program. A random order of ATP and peptide binding as well as that of ADP and phosphopeptide release was included. Time courses of HER2Peptide phosphorylation determined in Figure 4 by rapid quench are shown (filled circles). Simulations were performed using (A) 2.6 μM HKD and (B) 1.8 μM HCD (cf., 10 μM enzyme used in actual experiments).

groups in the analysis of other enzyme mechanisms and was thus chosen for simulations of the HER-2 phosphoryltransfer reactions (*67*−*69*).

Evaluation of Scheme 3 with the KinTekSim computer program using the experimentally determined values of Table 6 suggests that this model for the kinetic mechanism of HER-2 catalysis is consistent with the data (Figure 7). Furthermore, simulations performed using models wherein substrate binding (Scheme 3, steps one and two) and product release (steps five and six) occur in an ordered fashion or randomly were identical, suggesting that the order of these steps is inconsequential for proper data fitting. As noted above, the amplitude of the pre-steady-state burst experiments suggested that the concentration of enzyme active sites was approximately 10−15%. Importantly, computer modeling using the parameters of Table 6 can predict the experimental data *only if* the enzyme concentration entered is ∼20% of that used in the actual experiments. Hence, it is likely that a significant reason for our failure to observe a full-amplitude burst is due to the presence of inactive enzyme (∼80%). The remaining 10% decrease in amplitude can be accounted for by characteristics of the reaction kinetics (namely, a relatively slow rate of chemical catalysis compared to that of the rate-limiting step) (*62*). Thus, Scheme 3 and the values in Table 6 can be used to generate a minimal mechanism that is not only consistent with but also helps explain pre-steady-state observations.

Making the proper adjustments in enzyme concentration, simulation of steady-state experiments in which the rates for HER2Peptide phosphorylation are determined as a function of peptide concentration result in similar V_{max} values as those determined experimentally (0.5 μM s^{-1}). This analysis indicates that the kinetic constants in Table 6 can account for steady-state turnover of HER2Peptide. However, the K_m value (79 μM) obtained from these simulations is about 4-fold smaller than the experimentally determined value of 350 μM. As previously noted, since no direct measurements for HER2Peptide binding or dissociation have yet been conducted, the constraint placed on the values for the rate constants of step two (Scheme 3) was such that the ratio of the rate constants for peptide dissociation and association were approximated by the K_m value of HER2Peptide. This assumption may not necessarily be valid, however, since the true K_d value of a substrate is oftentimes not equal to its K_m. Indeed, the true K_d value of Kemptide for cAPK was determined by rapid quench methodologies to be 40-fold greater than its steady-state determined K_m value (*16*). Hence, the true K_d value of HER2Peptide is likely to be greater than its K_m.

We used kinetic simulations to model whether the conformational change (step four) proposed in Scheme 3 is necessary for data fitting, the HER-2 phosphoryltransfer reaction. The simulations were carried out in the presence and absence of this event. For these simulations, the rate-limiting step described by the linear phase of the rapid quench experiments was assigned to that of ADP release.

Hence, the association rate constant for ADP was similarly adjusted in order to maintain the K_d determined by stopped-flow studies. This adjustment translated to a 27% (for HKD) or 75% (for HCD) decrease in the rate constants determined by stopped-flow for mantADP, a magnitude which is quite substantial. The kinetic simulations of the pre-steady-state burst experiments for HKD and HCD *without* the rate-limiting conformational change tend to underestimate the burst phase and overestimate the steady-state phase (data not shown). Thus, as an initial attempt, these simulations may imply that HKD and HCD phosphorylate HER2Peptide with a rate-limiting conformational change however additional experiments are clearly necessary to substantiate this suggestion.

By altering individual rate constants while holding others constant, a user of the KinTekSim software can determine how such perturbations affect the overall reaction kinetics. This technique is particularly useful for understanding how variations in less-well-defined rate constants might affect the behavior of the proposed mechanism. Using this method, it was established that the precise values for the association and dissociation rate constants for the peptide substrate and product (steps two and five) do not affect proper data fitting, as long as these rates are not rate-limiting. Indeed, assigning dissociation rate constants for HER2Peptide using values as low as 17.5 s^{-1} (and association rate constant of 0.05 μM^{-1} s^{-1}, as stipulated by the K_m approximation of K_d) does not significantly impact the kinetic mechanism. These KinTekSim studies indicate that the kinetic mechanism for HER-2 phosphorylation of exogenous substrates as depicted in Scheme 3 can be used to predict experimentally determined time courses by global analysis. As other kinetically relevant steps become apparent through future studies, the mechanism of phosphoryltransfer can be expanded and simulated accordingly.

Comparison of the mechanism for the HER-2 tyrosine kinase phosphorylation of HER2Peptide (Scheme 3 and Table 6) with the mechanism reported for the classical serine/threonine kinase cAPK in the phosphorylation of Kemptide substrate (*17*−*19*) suggests a similarity in the overall mechanism. Most notably, substrate binding is followed by chemical catalysis and product release, and a conformational change is thought to contribute to the overall rate-limiting step. In either case, the mechanistic studies have shown that the chemical step is clearly not the step which limits the overall kinetic reaction pathway. These results are in contrast to studies with a nonreceptor tyrosine kinase, Csk (C-terminal src kinase) in which it has been suggested that the chemical step is rate-limiting and the transition state follows a dissociative pathway during phosphoryl transfer (*70*). However, Csk has not been subjected to a transient kinetic analysis to definitively establish the rate-limiting step.

Until now, only steady-state parameters have been determined for tyrosine kinases, and little has been done to uncover the mechanistic basis for the slower V_{max} seen in RTK phosphorylation relative to the faster serine/threonine kinases. At a chemical level, it has been proposed that the discrepancy between maximal velocities seen in phosphorylation of serine/threonine and tyrosine residues may be partially explained by the relative nucleophilicities of the attacking alkoxides (*71*). Consistent with this notion, Lee et al (*72*) have shown that cAPK phosphorylates an aromatic alcohol 120-fold slower than its primary alcohol counterpart. Furthermore, the observed differences in the cAPK steady-state parameters for these compounds was demonstrated to be due primarily to the inherent electron-withdrawing power of the aromatic nucleus, and alterations in nucleophilicity of the phenolic hydroxyl by electron-donating or withdrawing ring substituents predictably influenced K_m and V_{max} values of the respective compounds (*72*).

Indeed, while transient kinetic measurements of cAPK indicate that the actual step of chemistry occurs at 500−600 s^{-1} (*17*, *18*), our measurements suggest that this step occurs 2 orders of magnitude slower in HER-2. Significantly, however, HER-2 catalysis occurs one or 2 orders of magnitude more slowly than that of cAPK for each of the other measured steps [ATP and ADP association and dissociation, proposed conformational change(s), *as well as* chemistry] (*17*, *18*). How the HER-2 tyrosine kinase compares with the other tyrosine kinases must await the characterization of their mechanisms.

While further investigation (such as those using substrates with higher affinity or the use of phosphopeptides for characterization of the reverse reaction) may help to better define some of the kinetic parameters in Table 6, the current mechanistic study on the HER-2 tyrosine kinase provides a foundation from which to understand the effects of perturbations to the reaction system. For instance, the action of potential inhibitors can be determined mechanistically, and such information can be utilized for the directed synthesis of more specific and potent chemotherapeutics for HER-2 driven malignancies. The phosphorylation of natural HER-2 protein substrates may also be compared to that of HER2Peptide to determine the potential impact of protein substrate residues distant from the phosphorylatable tyrosine on kinase activity. Thus, these initial investigations of the HER-2 tyrosine kinase reaction provide a practical framework for addressing many issues at the mechanistic level.

REFERENCES

1. Coussens, L., Yang-Feng, T. L., Liao, Y. C., Chen, E., Gray, A., McGrath, J., Seeburg, P. H., Libermann, T. A., Schlessinger, J., and Francke, U. (1985) *Science 230*, 1132−1139.
2. Hanks, S. K., Quinn, A. M., and Hunter, T. (1988) *Science 241*, 42−52.
3. Johnson, L. N., Noble, M., and Owen, D. J. (1996) *Cell 85*, 149−156.
4. Shoji, S., Titani, K., Demaille, J. G., and Fischer, E. H. (1979) *J. Biol. Chem. 254*, 6211−6214.
5. DeBondt, H. L. D., Rosenblatt, J., Jancarik, J., Jones, H. D., Morgan, D. O., and Kim, S.-H. (1993) *Nature 363*, 595−602.
6. Hu, S.-H., Parker, M. W., Lei, J. Y., Wilce, M. C. J., Benian, G. M., and Kemp, B. E. (1994) *Nature 369*, 581−585.
7. Zhang, F., Strand, A., Robbins, D., Cobb, M. H., and Goldsmith, E. J. (1994) *Nature 367*, 704−711.
8. Owen, D. J., Noble, M. E., Garman, E. F., Papageorgiou, A. C., and Johnson, L. N. (1995) *Structure 3*, 467−482.
9. Goldberg, J., Nairn, A. C., and Kuriyan, J. (1996) *Cell 84*, 875−87.
10. Longenecker, K. L., Roach, P. J., and Hurley, T. D. (1996) *J. Mol. Biol. 257*, 618−631.
11. Hubbard, S., Wei, L., Ellis, L., and Hendrichson, W. A. (1994) *Nature 372*, 746−754.
12. Mohammadi, M., Schlessinger, J., and Hubbard, S. (1996) *Cell 86*, 577−587.
13. Yamaguchi, H., and Hendrickson, W. A. (1996) *Nature 384*, 484−489.

14. Sicheri, F., Moarefi, I., and Kuriyan, J. (1997) *Nature 385*, 602−609.
15. Xu, W., Harrison, S. C., and Eck, M. J. (1997) *Nature 385*, 595−602.
16. Grant, B. D., and Adams, J. A. (1996) *Biochemistry 35*, 2022−2029.
17. Lew, J., Taylor, S. S., and Adams, J. A. (1997) *Biochemistry 36*, 6717−6724.
18. Shaffer, J., and Adams, J. A. (1999) *Biochemistry 38*, 12072−12079.
19. Shaffer, J., and Adams, J. A. (1999) *Biochemistry 38*, 5572−5581.
20. Levitzki, A., and Gazit, A. (1995) *Science 24*, 267(5205), 1782−1788.
21. Natali, P. G., Nicotra, M. R., Digiesi, G., Cavaliere, R., Bigotti, A., Trizio, D., and Segatto, O. (1994) *Int. J. Cancer 56*, 341−346.
22. King, C. R., Kraus, M. H., and Aaronson, S. A. (1985) *Science 229*, 974−976.
23. Slamon, D. J., Clark, G. M., Wong, S. G., Levin, W. J., Ullrich, A., and McGuire, W. L. (1987) *Science 235*, 177−182.
24. Slamon, D. J., Godolphin, W., Jones, L. A., Holt, J. A., Wong, S. G., Keith, D. E., Levin, W. J., Stuart, S. G., Udove, J., and Ullrich, A., et al. (1989) *Science 244*, 707−712.
25. Paik, S. (1992) *Cancer Invest. 10*, 575−579.
26. Hynes, N. E., and Stern, D. F. (1994) *Biochim. Biophys. Acta 1198*, 165−184.
27. Gibbs, J. B., and Oliff, A. (1994) *Cell 79*, 193−198.
28. Bargmann, C. I., Hung, M.-C., and Weinberg, R. A. (1986) *Nature 319*, 226−230.
29. Yamamoto, T., Ikawa, S., Akiyama, T., Semba, K., Nomura, N., Miyajima, N., Saito, T., and Toyosha, K. (1986) *Nature 319*, 230−240.
30. Schechter, A. L., Stern, D. F., Vaidyanathan, L., Decker, S. J., Drebin, J. A., Grenne, M. I., and Weinberg, R. A. (1984) *Nature 312*, 513−516.
31. Ullrich, A., Coussens, L., Hayflick, J. S., Dull, T. J., Gray, A., Tam, A. W., Lee, J., Yarden, Y., Libermann, T. A., and Schlessinger, J., et al. (1984) *Nature 309*, 418−425.
32. Kraus, M. H., Issing, W., Miki, T., Popescu, N. C., and Aaronson, S. A. (1989) *Proc. Natl. Acad. Sci. U.S.A. 86*, 9193−9197.
33. Hanks, S. K., and Quinn, A. M. (1991) *Methods Enzymol. 200*, 38−62.
34. Plowman, G. D., Culouscou, J. M., Whitney, G. S., Green, J. M., Carlton, G. W., Foy, L., Neubauer, M. G., and Shoyab, M. (1993) *Proc. Natl. Acad. Sci. U.S.A. 90*, 1746−1750.
35. Akiyama, T., Matsuda, S., Namba, Y., Saito, Y., Toyshima, K., and Yamamoto, T. (1991) *Mol. Cell Biol. 11.2*, 833−842.
36. Bargmann, C. I., and Weinberg, R. A. (1988) *EMBO J 7*, 2043−2052.
37. Weiner, D. B., Kokai, Y., Wada, T., Cohen, J. A., Williams, W. V., and Greene, M. I. (1989) *Oncogene 4*, 1175−1183.
38. Baselga, J., Tripathy, D., Mendelsohn, J., Baughman, S., Benz, C., Dantis, L., Sklarin, N., Seidman, A., Hudis, D., Moore, J., Rosen, P., Twaddell, T., Henderson, I., and Norton, L. (1996) *J. Clin. Oncol. 14*, 737−744.
39. Cobleigh, M. A., Vogel, C. L., Tripathy, D., Robert, N., Scholl, S., Fehrenbacher, L., Paton, V., Shak, S., Lieberman, G., and Slamon, D. (1998) *Proc. Am. Soc. Clin. Oncol. 17*, 97a (Abstr. 376).
40. Pegram, M. D., Lipton, A., Hayes, D. F., Weber, B. L., Baselga, J. M., Tripathy, D., Baly, D., Baughman, S. A., Twaddell, T., Glaspy, J. A., and Slamon, D. J. (1998) *J. Clin. Oncol. 16*, 2659−2671.
41. Guy, P. M., Carraway, K. L., III, and Cerione, R. A. (1992) *J. Biol. Chem. 267*, 13851−13856.
42. Laemmli, U. K. (1970) *Nature 270*, 680−685.
43. Hiratsuka, T. (1983) *Biochim. Biophys. Acta 742*, 496−508.
44. Jameson, D. M., and Eccleston, J. F. (1997) *Methods Enzymol. 278*, 363−390.
45. Moore, K. J., and Lohman, T. M. (1994) *Biochemistry 33*, 14565−14578.
46. Songyang, Z., Blechner, S., Hoagland, N., Hoekstra, M. F., Piwnica-Worms, H., and Cantley, L. C. (1994) *Curr. Biol. 4*, 973−982.
47. Songyang, Z., Carraway, K. L., Eck, M. J., Harrison, S. C., Feldman, R. A., Mohammadi, M., Schlessinger, J., Hubbard, S. R., Smith, D. P., Eng, C., Lorenzo, M. J., Ponder, B. A. J., Mayer, B. J., and Cantley, L. C. (1995) *Nature 373*, 536.
48. Myers, J., LeVea, C., Smith, J., Kallen, R., Tung, L., and Greene, M. (1992) *Receptor 2*, 1−16.
49. Carpenter, G., King, L., Jr., and Cohen, S. (1979) *J. Biol. Chem. 254*, 4884−4891.
50. Herrera, R., Lebwohl, D., Garcia de Herreros, A., Kallen, R. G., and Rosen, O. M. (1988) *J. Biol. Chem. 263*, 5560−5568.
51. Wedegaertner, P. B., and Gill, G. N. (1989) *J. Biol. Chem. 264*, 11346−11353.
52. Foulkes, J. G., Chow, M., Gorka, C., Frackelton, A. R., Jr., and Baltimore, D. (1985) *J. Biol. Chem. 260*, 8070−8077.
53. Cadena, D. L., Chan, C. L., and Gill, G. N. (1994) *J. Biol. Chem. 269*, 260−265.
54. Bertics, P. J., Chen, W. S., Hubler, L., Lazar, C. S., Rosenfeld, M. G., and Gill, G. N. (1988) *J. Biol. Chem. 263*, 3610−3617.
55. Hsuan, J. J., Totty, N., and Waterfield, M. D. (1989) *Biochem. J. 262*, 659−663.
56. Ho, M., Bramson, H. N., Hansen, D. E., Knowles, J. R., and Kaiser, E. T. (1988) *J. Am. Chem. Soc. 110*, 2681−2683.
57. Weber, W., Bertics, P. J., and Gill, G. N. (1984) *J. Biol. Chem. 259* (23), 14631−14636.
58. Hubbard, S. R. (1997) *EMBO J. 16*, 5572−5581.
59. Posner, I., Engel, M., and Levitzki, A. (1992) *J. Biol. Chem. 267*, 20638−20647.
60. Kati, W. M., Johnson, K. A., Jerva, L. F., and Anderson, K. S. (1992) *J. Biol. Chem. 267*, 25988−25997.
61. Johnson, K. A. (1993) *Ann. Rev. Biochem. 62*, 685−713.
62. Johnson, K. A. (1992) *Enzymes 20*, 1−61.
63. Sherrill, J. M. (1997) *Biochemistry 36*, 5677−5684.
64. Bertics, P. J., and Gill, G. N. (1985) *J. Biol. Chem. 260* (27), 14642−14647.
65. Honegger, A. M., Dull, T. J., Szapary, D., Komoriya, A., Kris, R., Ullrich, A., and Schlessinger, J. (1988) *EMBO J. 7* (10), 3053−3060.
66. Johnson, K. A. (1995) *Methods Enzymol 249*, 38−61.
67. Barshop, B. A., Wrenn, R. F., and Frieden, C. (1983) *Anal.Biochem. 130*, 134−145.
68. Anderson, K. S., and Johnson, K. A. (1990) *Chem. Rev. 90*, 1131−1149.
69. Fierke, C., and Hammes, G. (1995) *Methods Enzymol. 249*, 3.
70. Cole, P. A., Sondhi, D., and Kim, K. (1999) *Pharmacol. Ther. 82*, 219−29.
71. Martin, B. L., Wu, D., Jakes, S., and Graves, D. J. (1990) *J. Biol. Chem. 265*, 7108−7111.
72. Lee, T. R., Niu, J., and Lawrence, D. S. (1994) *Biochemistry 33*, 4245−4250.
73. Segel, I. H. *Enzyme Kinetics: Behavior and Analysis of Rapid Equilibrium and Steady-State Enzyme Systems*. New York: John Wiley and Sons, Inc., 1975.

BI9924922